Abstracta

Ano XXIV - N. 06

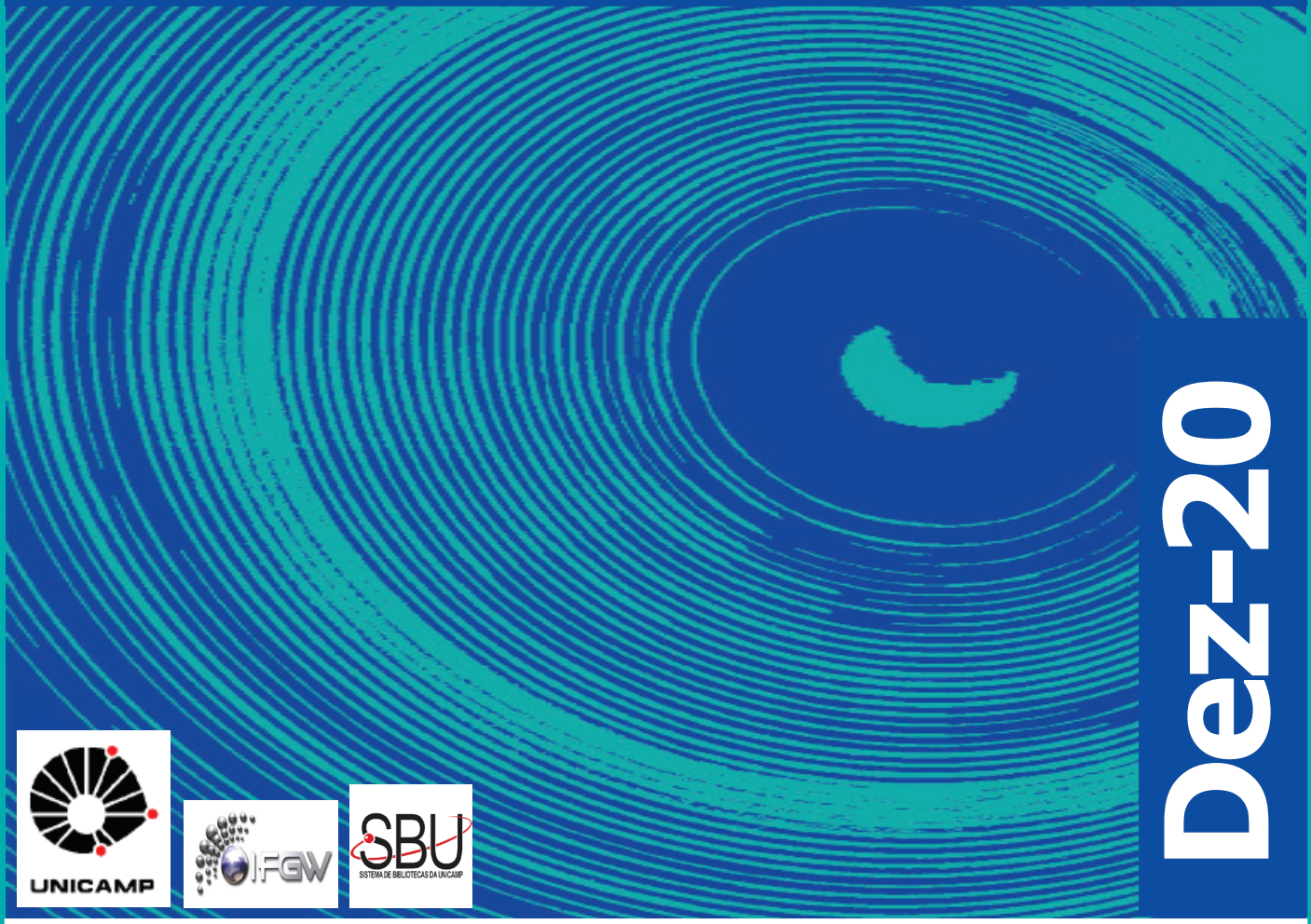

Dez-20

Artigos publicados - P294-2020 à P364-2020

Eventos publicados - P365-2020 à P366-2020

Patentes - Pa004-2020 à Pa006-2020

Defesas de Teses do IFGW - T015-2020 à T016-2020

Defesas e Qualificações do PECIM - Pe004-2020 à Pe006-2020

Artigos publicados

[P294-2020] "(Anti-)deuteron production in pp collisions at root s=13 TeV"

Acharya, S.; Acosta, F. T.; Adam, J.; **Albuquerque, D. S. D.*; Chinellato, D. D.*; De Souza, R. D.*; Takahashi, J.*;** et. al.; ALICE Collaboration

The study of (anti-)deuteron production in pp collisions has proven to be a powerful tool to investigate the formation mechanism of loosely bound states in high-energy hadronic collisions. In this paper the production of (anti-)deuterons is studied as a function of the charged particle multiplicity in inelastic pp collisions at root s = 13 TeV using the ALICE experiment. Thanks to the large number of accumulated minimum bias events, it has been possible to measure (anti-)deuteron production in pp collisions up to the same charged particle multiplicity (dN(ch)/d eta similar to 26) as measured in p-Pb collisions at similar centre-of-mass energies. Within the uncertainties, the deuteron yield in pp collisions resembles the one in p-Pb interactions, suggesting a common formation mechanism behind the production of light nuclei in hadronic interactions. In this context the measurements are compared with the expectations of coalescence and statistical hadronisation models (SHM).

EUROPEAN PHYSICAL JOURNAL C 80[9], 889, 2020. DOI: 10.1140/epjc/s10052-020-8256-4

[P295-2020] "A Search for Ultra-high-energy Neutrinos from TXS 0506+056 Using the Pierre Auger Observatory"

Aab, A.; Abreu, P.; Aglietta, M.; **Chinellato, J. A.*; Daniel, B.*; Diaz Castro, M. L.*; Dobrigkeit, C.*; Fauth, A. C.*; Muller, M. A.*; Pereira, L. A. S.*;** et. al.; Pierre Auger Collaboration

Results of a search for ultra-high-energy neutrinos with the Pierre Auger Observatory from the direction of the blazar TXS 0506+056 are presented. They were obtained as part of the follow-up that stemmed from the detection of high-energy neutrinos and gamma rays with IceCube, Fermi-LAT, MAGIC, and other detectors of electromagnetic radiation in several bands. The Pierre Auger Observatory is sensitive to neutrinos in the energy range from 100 PeV to 100 EeV and in the zenith-angle range from = 60 degrees to = 95 degrees, where the zenith angle is measured from the vertical direction. No neutrinos from the direction of TXS 0506+056 have been found. The results were analyzed in three periods: one of 6 months around the detection of IceCube-170922 A, coinciding with a flare period of TXS 0506+056, a second one of 110 days during which the IceCube collaboration found an excess of 13 neutrinos from a direction compatible with TXS 0506+056, and a third one from 2004 January 1 up to 2018 August 31, over which the Pierre Auger Observatory has been taking data. The sensitivity of the Observatory is addressed for different spectral indices by considering the fluxes that would induce a single expected event during the observation period. For indices compatible with those measured by the IceCube collaboration the expected number of neutrinos at the Observatory is well below one. Spectral indices as hard as 1.5 would have to apply in this energy range to expect a single event to have been detected.

ASTROPHYSICAL JOURNAL 902[2], 105, 2020. DOI: 10.3847/1538-4357/abb476

[P296-2020] "Azimuthal correlations of prompt D mesons with charged particles in pp and p-Pb collisions at root s(NN)=5.02 TeV"

Acharya, S.; Acosta, F. T.; Adam, J.; **Albuquerque, D. S. D.*; Chinellato, D. D.*; De Souza, R. D.*; Takahashi, J.*;** et. al.; ALICE Collaboration

The measurement of the azimuthal-correlation function of prompt D mesons with charged particles in pp collisions at root s = 5.02 TeV and p-Pb collisions at root s(NN) = 5.02 TeV with the ALICE detector at the LHC is reported. The D-0, D+, and D*+ mesons, together with their charge conjugates, were reconstructed at midrapidity in the transverse momentum interval 3 < p(T) < 24 GeV/c and correlated with charged particles having p(T) > 0.3 GeV/c and pseudorapidity vertical bar eta vertical bar < 0.8. The properties of the correlation peaks appearing in the near- and away-side regions (for Delta phi approximate to 0 and Delta phi approximate to pi, respectively) were extracted via a fit to the azimuthal correlation functions. The shape of the correlation functions and the near- and away--side peak features are found to be consistent in pp and p-Pb collisions, showing no modifications due to nuclear effectswithin uncertainties. The results are compared with predictions from Monte Carlo simulations performed with the PYTHIA, POWHEG+PYTHIA, HERWIG, and EPOS 3 event generators.

EUROPEAN PHYSICAL JOURNAL C 80[10], 979, 2020. DOI: 10.1140/epjc/s10052-020-8118-0

[P297-2020] "Complete and commented translation of Guillaume's 1896 paper on the temperature of space"

Assis, A. K. T.*; Neves, M. C. D.

Charles Edouard Guillaume (1861-1928) was a Swiss physicist who received the 1920 Nobel Prize in physics for his precision measurements and discovery of anomalies in nickel steel alloys. In this work, we present a complete and commented translation of his remarkable article of 1896 on the temperature of interstellar space. The importance of this work is that it is the oldest estimate known to us of the temperature acquired by a black body, which is in interstellar space far from other stars. This temperature was presumed to be due to an equilibrium state in which the radiation received by this body from the stars around it would be equal to the radiation emitted by the body. He arrived at a temperature of 5:6 K, regarding this figure as an upper limit on the effect he was seeking to estimate. In 1926, Arthur Eddington (1882-1944) arrived at a temperature of 3:18 K, utilizing essentially the same procedure but with better data.

AMERICAN JOURNAL OF PHYSICS 88[12], 1140-1144, 2020. DOI: 10.1119/10.0001775

[P298-2020] "Constraining the Chiral Magnetic Effect with charge-dependent azimuthal correlations in Pb-Pb collisions at root s(NN)=2.76 and 5.02 TeV"

Acharya, S.; Acosta, F. T.; Adam, J.; **Albuquerque, D. S. D.*; Chinellato, D. D.*; De Souza, R. D.*; Takahashi, J.*;** et. al.; ALICE Collaboration

Systematic studies of charge-dependent two- and three-particle correlations in Pb-Pb collisions at root s(NN) = 2.76 and 5.02 TeV used to probe the Chiral Magnetic Effect (CME) are presented. These measurements are performed for charged particles in the pseudorapidity (eta) and transverse momentum (p(T)) ranges |eta| < 0.8 and 0.2 < p(T) < 5 GeV/c. A significant charge-dependent signal that becomes more pronounced for peripheral collisions is reported for the CME-sensitive correlators gamma(1, 1) = < cos(phi(alpha) + phi(beta) - 2 psi(2))> and gamma(1, - 3) = < cos(phi(alpha) - 3 phi(beta) + 2 psi(2))>. The results are used to estimate the contribution of background effects, associated with local charge conservation coupled to anisotropic flow modulations, to measurements of the CME.

A blast-wave parametrisation that incorporates local charge conservation tuned to reproduce the centrality dependent background effects is not able to fully describe the measured gamma(1,1). Finally, the charge and centrality dependence of mixed-harmonics three-particle correlations, of the form gamma(1, 2) = < cos(phi(alpha) + 2 phi(beta) - 3 psi(3))>, which are insensitive to the CME signal, verify again that background contributions dominate the measurement of gamma(1,1).

JOURNAL OF HIGH ENERGY PHYSICS 9, 160, 2020. DOI: 10.1007/JHEP09(2020)160

[P299-2020] "Constraining visible neutrino decay at KamLAND and JUNO"

Porto-Silva, Y. P.*; Prakash, S.*; Peres, O. L. G.*; Nunokawa, H.; Minakata, H.

We study visible neutrino decay at the reactor neutrino experiments KamLAND and, JUNO. Assuming the Majoron model of neutrino decay, we obtain constraints on the couplings between Majoron and neutrino as well as on the lifetime/mass of the most massive neutrino state i.e., tau(3)/m(3) or tau(2)/m(2), respectively, for the normal or the inverted mass orderings. We obtain the constraints on the lifetime tau(2)/m(2)>= 1.4x10(-9) s/eV in the inverted mass ordering for both KamLAND and JUNO at 90% CL. In the normal ordering in which the bound can be obtained for JUNO only, the constraint is milder than the inverted ordering case, tau(3)/m(3) >= 1.0 x 10(-1)0 s/eV at 90% CL. We find that the dependence of lightest neutrino mass (= m(lightest)), m(1)(m(3)) for the normal (inverted) mass ordering, on the constraints for the different types of couplings (scalar or pseudo-scalar) is rather strong, but the m(lightest) dependence on the lifetime/mass bound is only modest.

EUROPEAN PHYSICAL JOURNAL C 80[10], 999, 2020. DOI: 10.1140/epjc/s10052-020-08573-9

[P300-2020] "Constraints on the Physical Properties of GW190814 through Simulations Based on DECam Follow-up Observations by the Dark Energy Survey"

Morgan, R.; Soares-Santos, M.; Annis, J.; **Sobreira, F.***; et. al.

On 2019 August 14, the LIGO and Virgo Collaborations detected gravitational waves from a black hole and a 2.6 solar mass compact object, possibly the first neutron star-black hole merger. In search of an optical counterpart, the Dark Energy Survey (DES) obtained deep imaging of the entire 90% confidence level localization area with Blanco/DECam 0, 1, 2, 3, 6, and 16 nights after the merger. Objects with varying brightness were detected by the DES Pipeline, and we systematically reduced the candidate counterparts through catalog matching, light-curve properties, host-galaxy photometric redshifts, Southern Astrophysical Research spectroscopic follow-up observations, and machine-learning-based photometric classification. All candidates were rejected as counterparts to the merger. To quantify the sensitivity of our search, we applied our selection criteria to full light-curve simulations of supernovae and kilonovae as they would appear in the DECam observations. Because the source class of the merger was uncertain, we utilized an agnostic, three-component kilonova model based on tidally disrupted neutron star (NS) ejecta properties to quantify our detection efficiency of a counterpart if the merger included an NS. We find that, if a kilonova occurred during this merger, configurations where the ejected matter is greater than 0.07 solar masses, has lanthanide abundance less than 10(-8.56), and has a velocity between 0.18cand 0.21care disfavored at the 2 sigma level. Furthermore, we estimate that our background reduction methods are capable of associating gravitational wave signals with a detected electromagnetic counterpart at the 4 sigma level in 95% of future follow-up observations.

ASTROPHYSICAL JOURNAL 901[1], 83, 2020. DOI: 10.3847/1538-4357/abafaa

[P301-2020] "Crystal imperfections in ice I-h"

Koning, M. de*

In this paper, we present an overview of crystal imperfections in ice I-h. Due to its molecular nature, the fundamental asymmetry of the hydrogen bond, and proton disorder, crystal defects in this condensed form of water reveal a complexity not usually seen in atomic crystalline solids. The discussion is organized in terms of the spatial extent of the defects. We start with zero-dimensional imperfections such as the molecular vacancy and interstitial, Bjerrum, and ionic defects, as well as possible defect complexes that can be formed from them. Subsequently, we turn to the properties of dislocations, which are the one-dimensional disturbances that carry plastic deformation in crystalline solids. Finally, we discuss two-dimensional defects such as stacking faults and grain boundaries and discuss to what extent the latter are similar to other interfaces in ice I-h such as the free surface. We conclude with an outlook at the road ahead, discussing future challenges toward understanding the role of crystal defects in the macroscopic behavior of ice I-h.

JOURNAL OF CHEMICAL PHYSICS 153[11], 110902, 2020. DOI: 10.1063/5.0019067

[P302-2020] "Electronic, optical and thermoelectric properties of boron-doped nitrogenated holey graphene"

Tromer, R. M*.; Freitas, A.; Felix, I. M.; Mortazavi, B.; Machado, L. D.; Azevedo, S.; Pereira, L. F. C.

We employ first principles calculations to investigate the electronic, optical, and thermoelectric properties of ten boron-doped nitrogenated holey graphene (NHG) monolayers. We find that most of the proposed structures remain stable duringab initiomolecular dynamics simulations, in spite of their increased formation energies. Density functional theory calculations employing a hybrid functional predict band gaps ranging from 0.73 eV to 2.30 eV. In general, we find that boron doping shifts optical absorption towards the visible spectrum, and also reduces light reflection in this region. On the other hand, the magnitude of optical absorption coefficients are reduced. Regarding the thermoelectric properties, we predict that boron doping can enhance the figure of meritZTof NHG by up to 55%. Our results indicate that boron-doped NHG monolayers may find application in solar cells and thermoelectric devices.

PHYSICAL CHEMISTRY CHEMICAL PHYSICS 22[37], 21147-21157 , 2020. DOI: 10.1039/d0cp02869j

[P303-2020] "Elementary Charge and Neutrino's Mass from Planck Length"

Carneiro, S.*

It is shown that the postulation of a minimum length for the horizons of a black hole leads to lower bounds for the electric charges and magnetic moments of elementary particles. If the minimum length has the order of the Planck scale, these bounds are given, respectively, by the electronic charge and by mu similar to 10(-21)mu(B). The latter implies that the masses of fundamental particles are bounded above by the Planck mass, and that the smallest non-zero neutrino mass is m(nu) similar to 10(-2) eV. A precise estimation in agreement to the area quantisation of Loop Quantum Gravity predicts a mass for the lightest massive state in concordance with flavor oscillation measurements, and a Barbero-Immirzi parameter in accordance to horizon entropy estimations.

FOUNDATIONS OF PHYSICS 50[11], 1376-1381, 2020. DOI: 10.1007/s10701-020-00383-z

[P304-2020] "Enhanced catalytic performance of CuFeS2 chalcogenide prepared by microwave-assisted route for photo-Fenton oxidation of emerging pollutant in water"

Salla, J. da S.; Dotto, G. L.; Hotza, D.; **Landers, R.*;** Martinello, K. B. de; Foletto, E. L.

In this work, CuFeS2 chalcogenide powders were easily produced by conventional and microwave methods, and for the first time, the influence of synthesis route on their properties and consequent catalytic activity in the photo-Fenton reaction was investigated. X-ray diffraction, N-2 adsorption-desorption isotherms, Fourier-transform infrared spectroscopy, transmission and scanning electron microscopy, energy dispersive X-ray spectroscopy and X-ray photoelectron spectroscopy were employed to characterize and point out the main properties and differences among samples. The CuFeS2 particles were used as catalysts for tartrazine dye degradation by the photo-Fenton reaction under visible irradiation. The results showed that the CuFeS2 prepared by microwaveassisted method (CuFeS2-MW) present higher crystallinity, higher concentration of Fe2+ on its surface and remarkable catalytic activity, reaching 99.1% of tartrazine decolorization and 87.3% of mineralization, at a rate twice as fast as CuFeS2 prepared by the conventional method. The catalyst showed high catalytic efficiency and stability during the reaction after five recycles. The hydroxyl radical was revealed to be the reactive species responsible for tartrazine degradation. A mechanism was proposed to elucidate how these free radicals are generated from the catalytic decomposition of H2O2 by CuFeS2-MW.

JOURNAL OF ENVIRONMENTAL CHEMICAL ENGINEERING 8[5], 104077, 2020. DOI: 10.1016/j.jece.2020.104077

[P305-2020] "Evolution of the magnetic properties in the antiferromagnet Ce2RhIn8 simultaneously doped with Cd and Ir"

Christovam, D. S.*; Freitas, G. S.*; Piva, M. M.*; Souza, J. C.*; Malcolms, M. O.*; Canton, O. L.; Leao, J. B.; Ratcliff, W.; Lynn, J. W.; **Adriano, C.*; Pagliuso, P. G.***

We report the evolution of the magnetic properties of Ce2Rh1--xIrxIn8-yCdy single crystals. In particular, for Ce2Rh0.5Ir0.5In8 (T-N = 2.0 K) and Ce2Rh0.5Ir0.5In7.79Cd0.21(T-N = 4.2 K), we have solved the magnetic structure of these compounds using single-crystal neutron magnetic diffraction experiments. Taking the magnetic structure of the Ce2RhIn8 heavy-fermion antiferromagnet as a reference, we have identified no changes in the q =(1/2, 1/2, 0) magnetic wave vector; however, the direction of the ordered Ce3+ moments rotates toward the ab plane, under the influence of both dopants. By constraining the analysis of the crystalline electric field (CEF) with the experimental ordered moment's direction and high--temperature magnetic-susceptibility data, we have used a mean-field model with tetragonal CEF and exchange interactions to gain insight into the CEF scheme and anisotropy of the CEF ground-state wave function when Cd and Jr are introduced into Ce2RhIn8. Consistent with previous work, we find that Cd doping in Ce2RhIn8 tends to rotate the magnetic moment toward the ab plane and lower the energy of the CEF excited states' levels. Interestingly, the presence of Jr also rotates the magnetic moment towards the ab plane although its connection to the CEF overall splitting evolution for the y = 0 samples may not be straightforward. These findings may shed light on the origin of the disordered spin-glass phase on the Jr-rich side of the phase diagram and also indicate that the Ce2MIn8 compounds may not follow exactly the same Rh--Ir CEF effects trend established for the CeMIn5 compounds.

PHYSICAL REVIEW B 102[19], 195137, 2020. DOI: 10.1103/PhysRevB.102.195137

[P306-2020] "Femtosecond fragmentation of CS2 after sulfur 1s ionization: interplay between Auger cascade decay, charge delocalization, and nuclear motion"

Granas, O.; Mocellin, A.; **Cardoso, E. S.***; Burmeister, F.; Caleman, C.; Bjorneholm, O.; **Brito, A. N. de***

We present a combined experimental and theoretical study of the fragmentation of molecular CS2 after sulfur 1s Auger cascade decay, consisting of electron-multi-ion coincidence spectra of charged fragments and theoretical simulations combining density functional theory and molecular dynamics. On the experimental side, a procedure for a complete determination of all sets of ions formed is described. For many of the fragmentation channels, we observed a higher charge in one of the sulfur atoms than the other atoms. Based on these observations and the theoretical simulations where the time scale of the nuclear motion and decay is taken into account, we propose that KLL Auger decay after the 1s core hole creation, via 2p double hole states, results in highly charged and strongly repulsive states with one localized core hole. These localized core holes are sufficiently long-lived that some will decay after fragmentation of the molecular ion, thereby efficiently impeding charge exchange between the fragments.

JOURNAL OF PHYSICS B-ATOMIC MOLECULAR AND OPTICAL PHYSICS 53[24], 244007, 2020. DOI: 10.1088/1361-6455/abc45d

[P307-2020] "First Cosmology Results using Supernovae Ia from the Dark Energy Survey: Survey Overview, Performance, and Supernova Spectroscopy"

Smith, M.; D'Andrea, C. B.; Sullivan, M.; **Sobreira, F.***; et. al.

We present details on the observing strategy, data-processing techniques, and spectroscopic targeting algorithms for the first three years of operation for the Dark Energy Survey Supernova Program (DES-SN). This five-year program using the Dark Energy Camera mounted on the 4 m Blanco telescope in Chile was designed to discover and follow supernovae (SNe) Ia over a wide redshift range (0.05 z < 1.2) to measure the equation-of-state parameter of dark energy. We describe the SN program in full: strategy, observations, data reduction, spectroscopic follow-up observations, and classification. From three seasons of data, we have discovered 12,015 likely SNe, 308 of which have been spectroscopically confirmed, including 251 SNe Ia over a redshift range of 0.017 z < 0.85. We determine the effective spectroscopic selection function for our sample and use it to investigate the redshift-dependent bias on the distance moduli of SNe Ia we have classified. The data presented here are used for the first cosmology analysis by DES-SN ("DES-SN3YR"), the results of which are given in Dark Energy Survey Collaboration et al. The 489 spectra that are used to define the DES-SN3YR sample are publicly available at.

ASTRONOMICAL JOURNAL 160[6], 267, 2020. DOI: 10.3847/1538-3881/abc01b

[P308-2020] "Generation of coherent phonons via a cavity enhanced photonic lambda scheme"

Bourhill, J.; **Carvalho, N. C.***; Goryachev, M.; Galliou, Serge; Tobar, M. E.

We demonstrate the generation of coherent phonons in a quartz bulk acoustic wave (BAW) resonator through the photoelastic properties of the crystal, via coupling to a microwave cavity enhanced by a photonic lambda scheme. This is achieved by imbedding a single crystal BAW resonator between the post and the adjacent wall of a microwave re-entrant cavity resonator. This 3D photonic lumped LC resonator at the same time acts as the electrode of a BAW phonon resonator and allows the direct readout of coherent phonons via the linear piezoelectric response of the quartz. A microwave pump, omega(p), is tuned to the cavity resonance omega(0), while a probe frequency, omega(probe), is detuned and varied around the red and blue detuned values with respect to the BAW phonon frequency, Omega(m). The pump and probe power dependence of the generated phonons unequivocally determines the process to be electrostrictive, with the phonons produced at the difference frequency between the pump and the probe, with no back action effects involved. Thus, the phonons are created without threshold and can be considered analogous to a passive coherent population trapped maser scheme.

APPLIED PHYSICS LETTERS 117[16], 164001, 2020. DOI: 10.1063/5.0023624

[P309-2020] "Global baryon number conservation encoded in net-proton fluctuations measured in Pb-Pb collisions at root s(NN)=2.76TeV"

Acharya, S.; Adamova, D.; Adler, A.; **Albuquerque, D. S. D.*; Chinellato, D. D.*; Takahashi, J.***; et. al.; ALICE Collaboration

Experimental results are presented on event-by-event net--proton fluctuation measurements in Pb-Pb collisions at root s(NN)= 2.76 TeV, recorded by the ALICE detector at the CERN LHC. These measurements have as their ultimate goal an experimental test of Lattice QCD (LQCD) predictions on second and higher order cumulants of net-baryon distributions to search for critical behavior near the QCD phase boundary. Before confronting them with LQCD predictions, account has to be taken of correlations stemming from baryon number conservation as well as fluctuations of participating nucleons. Both effects influence the experimental measurements and are usually not considered in theoretical calculations. For the first time, it is shown that event- by-event baryon number conservation leads to subtle long-range correlations arising from very early interactions in the collisions.

PHYSICS LETTERS B 807, 135564, 2020. DOI: 10.1016/j.physletb.2020.135564

[P310-2020] "Graphene-based nanoscale version of da Vinci's reciprocal structures"

Fonseca, A. F.*; Galvão, D. S.*

A reciprocal structure (RS) is a mechanical resistant structure formed by a set of self-supporting elements satisfying certain conditions of structural reciprocity (SR). The first condition is that each element of the structure has to support and be supported by the others. The second condition is that these functions cannot occur in the same part of the element. These two properties make beams and two-dimensional materials very much appropriate to build RSs. Commonly seen in floors or roofs, SR is also present in art, religious symbols, and decorative objects. Da Vinci has drawn several examples of such RSs. Here, thermal stability and mechanical resistance against impacts of simple nano versions of da Vinci's RSs based on graphene nanoribbons, were investigated through fully atomistic molecular dynamics (MD) simulations. We considered structures with three and four joins with and without RS topologies. Our MD results showed that 3-fold RSs are not thermally stable and that the 4-fold RSs can become thermally stable as long as the graphene nanoribbons have their external extremities fixed and either are not lengthy or have a kind of notch at the nanoribbons junctions. For these thermally stable structures, our results show that those with RS topologies are more impact resistant than those without SR, despite the fact that the used graphene nanoribbons are highly pliable. We discuss these results in terms of the number of joins, energy absorption, and stress on the structures. We discuss possible applications in nanoengineering.

COMPUTATIONAL MATERIALS SCIENCE 187[1], 110105, 2020. DOI: 10.1016/j.commatsci.2020.110105

[P311-2020] "Hydrodynamics of two-dimensional compressible fluid with broken parity: Variational principle and free surface dynamics in the absence of dissipation"

Abanov, A. G.; Can, T.; Ganeshan, S.; **Monteiro, G. M.***

We consider an isotropic compressible nondissipative fluid with broken parity subject to free surface boundary conditions in two spatial dimensions. The hydrodynamic equations describing the bulk dynamics of the fluid and the free surface boundary conditions depend explicitly on the parity-breaking nondissipative odd viscosity term. We construct an effective action which gives both bulk hydrodynamic equations and free surface boundary conditions. The free surface boundary conditions require an additional boundary term in the action which resembles a 1 + 1D chiral boson field coupled to the background geometry. We solve the linearized hydrodynamic equations for the deep water case and derive the dispersion of chiral surface waves. We show that in the long-wavelength limit the flow profile exhibits an oscillating vortical boundary layer near the free surface. The layer thickness is controlled by the ratio between the odd viscosity (nu(o)) and the sound velocity (c(s)), delta similar to nu(o)/c(s). In the incompressible limit, c(s) -> infinity, the vortical boundary layer becomes singular with the vorticity within the layer diverging as omega similar to c(s). The boundary layer is formed by odd viscosity coupling the divergence of velocity del center dot nu to vorticity del x nu. It results in nontrivial chiral free surface dynamics even in the absence of external forces. The structure of the odd-viscosity-induced boundary layer is very different from the conventional free surface boundary layer associated with dissipative shear viscosity.

PHYSICAL REVIEW FLUIDS 5[10], 104802, 2020. DOI: 10.1103/PhysRevFluids.5.104802

[P312-2020] "Influence of the Flow Rate in an Automated Microfluidic Electronic Tongue Tested for Sucralose Differentiation"

Braunger, M. L.*; Fier, I.; **Shimizu, F. M.*;** Barros, A. de; **Rodrigues, V.*; Riul Júnior, A.***

Incorporating electronic tongues into microfluidic devices brings benefits as dealing with small amounts of sample/discharge. Nonetheless, such measurements may be time-consuming in some applications once they require several operational steps. Here, we designed four collinear electrodes on a single printed circuit board, further comprised inside a straight microchannel, culminating in a robust e-tongue device for faster data acquisition. An analog multiplexing circuit automated the signal's routing from each of the four sensing units to an impedance analyzer. Both instruments and a syringe pump are controlled by dedicated software. The automated e-tongue was tested with four Brazilian brands of liquid sucralose-based sweeteners under 20 different flow rates, aiming to systematically evaluate the influence of the flow rate in the discrimination among sweet tastes sold as the same food product.

All four brands were successfully distinguished using principal component analysis of the raw data, and despite the nearly identical sucralose-based taste in all samples, all brands' significant distinction is attributed to small differences in the ingredients and manufacturing processes to deliver the final food product. The increasing flow rate improves the analyte's discrimination, as the silhouette coefficient reaches a plateau at similar to 3 mL/h. We used an equivalent circuit model to evaluate the raw data, finding a decrease in the double--layer capacitance proportional to improvements in the samples' discrimination. In other words, the flow rate increase mitigates the formation of the double-layer, resulting in faster stabilization and better repeatability in the sensor response.

SENSORS 20[21], 6194, 2020. DOI: 10.3390/s20216194

[P313-2020] "Influence of the Vibrational Modes from the Organic Moieties in 2D Lead Halides on Excitonic Recombination and Phase Transition"

Moral, R. F.; Germino, J. C.; Bonato, L. G.; **Almeida, D. B.***; Therezio, E. M.; Atvars, T. D. Z.; Stranks, S. D.; Nome, R. A.; Nogueira, A. F.

2D metal halide semiconductors have been intensively studied in the past few years due to their unique optical properties and potential for new-generation photonic devices. Despite the large number of recent works, this class of materials is still in need of further understanding due to their complex structural and optical characteristics. In this work, a molecular-level explanation for the dual band emission in the 2D (C4H9NH3)(2)PbI4 in its bulk form is presented, demonstrating that this feature is caused by a strong exciton-phonon coupling. Temperature-dependent photoluminescence with Raman and IR spectroscopies reveals that vibrations involving the C-NH3+ butylammonium polar head are responsible for this exciton-phonon coupling. Additionally, experimental shifts in the mean phonon frequencies coupled with the electronic excitation, combined with a theoretical model, show that these vibrational modes present a soft-mode behavior in the phase transition of this material.

ADVANCED OPTICAL MATERIALS 2001431, 2020. DOI: 10.1002/adom.202001431

[P314-2020] "Insights into the nature of optically active defects of ZnO"

Cabral, L.*; Lopez-Richard, V.; Silva, J. L. F. da; Marques, G. E.; Lima, M. P.; Onofre, Y. J.; Teodoro, M. D.; Godoy, M. P. F. de

ZnO is a wide bandgap semiconductor in which point and extended defects tune its optoelectronic properties, and the identification of essential microscopic ingredients for such a tunning is a challenging task. In this work, we combine experimental techniques with theoretical calculations at the atomistic level to investigate a variety of neutral and charged point defects along with their response to thermal treatment by optical and transport measurements. We obtain photoluminescence spectra compatible with simulations of Zn vacancies, oxygen interstitials, and complexes combining vacancies of Zn and O. Annealing is an effective way to neutralize the oxygen interstitials, being an effective mechanism to control the ZnO optoelectronic properties. The photosensitive behavior is explored in temperature-dependent electrical responses under different cooling-down modes. The role of both, extended and point defects, in the photoexcitation with energies below and above the bandgap is also discussed.

JOURNAL OF LUMINESCENCE 227, 117536, 2020. DOI: 10.1016/j.jlumin.2020.117536

[P315-2020] "Integrated Photonic Platform for Robust Differential Refractive Index Sensor"

Moras, A. L.*; Silva, V.; **Souza, M. C. M. M.***; Cirino, G. A.; **Von Zuben, A. A. G.***; Barea, L. A. M.; **Frateschi, N. C.***

We demonstrate an integrated photonic platform comprising a refractive index (RI) sensor based on Photonic Molecule (PM) that effectively mitigates the influence of environmental perturbations using a differential measurement scheme while providing high quality-factor (Q) resonances. The RI sensor consists of a partially unclad microdisk resonator coupled to an external clad microring resonator fabricated on silicon-on--insulator (SOI) platform. We report a RI sensitivity of 24 nm/RIU, achieving a limit of detection (LOD) of 1.7 x 10(-3) refractive index units (RIU) with improved stability for an operation range of 0.15 RIU in a compact footprint of 40 x 40 mu m(2), representing an important solution for real-life applications in which measurement conditions are not easily controllable.

IEEE PHOTONICS JOURNAL 12[5], 6802910, 2020. DOI: 10.1109/JPHOT.2020.3024856

[P316-2020] "Investigation into the event-activity dependence of gamma(nS) relative production in proton-proton collisions at root s=7 TeV"

Sirunyan, A. M.; Tumasyan, A.; Adam, W.; **Chinellato, J. A.*; Tonelli Manganote, E. J.***; et. al.; CMS Collaboration

The ratios of the production cross sections between the excited gamma(2S) and gamma(3S) mesons and the gamma(1S) ground state, detected via their decay into two muons, are studied as a function of the number of charged particles in the event. The data are from proton-proton collisions at root s = 7TeV, corresponding to an integrated luminosity of 4.8 fb(-1), collected with the CMS detector at the LHC. Evidence of a decrease in these ratios as a function of the particle multiplicity is observed, more pronounced at low transverse momentum p(T)(mu mu). For gamma(nS) mesons with p(T)(mu mu) > 7 GeV, where most of the data were collected, the correlation with multiplicity is studied as a function of the underlying event transverse sphericity and the number of particles in a cone around the gamma(nS) direction. The ratios are found to be multiplicity independent for jet--like events. The mean p(T)(mu mu) values for the gamma(nS) states as a function of particle multiplicity are also measured and found to grow more steeply as their mass increases.

JOURNAL OF HIGH ENERGY PHYSICS 11, 001, 2020. DOI: 10.1007/JHEP11(2020)001

[P317-2020] "J/psi elliptic and triangular flow in Pb-Pb collisions at root s(NN)=5.02 TeV"

Acharya, S.; Adamova, D.; Adler, A.; **Albuquerque, D. S. D.*; Chinellato, D. D.*; Takahashi, J.***; et. al.; ALICE Collaboration

The inclusive J/psi (v(2)) and triangular (v(3)) flow coefficients measured at forward rapidity (2.5 < y < 4) and the v2 measured at midrapidity (vertical bar y vertical bar < 0.9) in Pb-Pb collisions at root s(NN) = 5.02TeV using the ALICE detector at the LHC are reported. The entire Pb-Pb data sample collected during Run 2 is employed, amounting to an integrated luminosity of 750 mu b(-1) at forward rapidity and 93 mu b(-1) at midrapidity. The results are obtained using the scalar product method and are reported as a function of transverse momentum p(T) and collision centrality. At midrapidity, the J psi v(2) is in agreement with the forward rapidity measurement. The centrality averaged results indicate a positive J/psi v(3) with a significance of more than 5 sigma at forward rapidity in the p(T) range 2 < p(T) < 5 GeV/c.

The forward rapidity v(2), v(3), and v(3)/v(2) results at low and intermediate p(T) (p(T) < 8 GeV/c) exhibit a mass hierarchy when compared to pions and D mesons, while converging into a species-independent curve at higher p(T). At low and intermediate p(T), the results could be interpreted in terms of a later thermalization of charm quarks compared to light quarks, while at high p(T), path-length dependent effects seem to dominate. The J/psi v(2) measurements are further compared to a microscopic transport model calculation. Using a simplified extension of the quark scaling approach involving both light and charm quark flow components, it is shown that the D-meson vn measurements can be described based on those for charged pions and J/flow.

JOURNAL OF HIGH ENERGY PHYSICS 10, 141, 2020. DOI: 10.1007/JHEP10(2020)141

[P318-2020] "J/psi production as a function of charged-particle multiplicity in p-Pb collisions at root s(NN)=8.16 TeV"

Acharya, S.; Adamova, D.; Adler, A.; **Albuquerque, D. S. D.*; Chinellato, D. D.*; Takahashi, J.***; et. al.; ALICE Collaboration

Inclusive J/psi yields and average transverse momenta in p-Pb collisions at a center-of-mass energy per nucleon pairs root s(NN) = 8.16 TeV are measured as a function of the charged--particle pseudorapidity density with ALICE. The J/psi mesons are reconstructed at forward (2.03< y(cms) <3.53) and backward (-4.46< y(cms) < -2.96) center-of-mass rapidity in their dimuon decay channel while the charged-particle pseudorapidity density is measured around midrapidity. The J/psi yields at forward and backward rapidity normalized to their respective average values increase with the normalized charged-particle pseudorapidity density, the former showing a weaker increase than the latter. The normalized average transverse momenta at forward and backward rapidity manifest a steady increase from low to high charged-particle pseudorapidity density with a saturation beyond the average value.

JOURNAL OF HIGH ENERGY PHYSICS 9, 162, 2020. DOI: 10.1007/JHEP09(2020)162

[P319-2020] "Limitations imposed by complementarity"

Steinhoff, F. E. S.; **Oliveira, M. C.* de**

Complementarity is one of the main features of quantum physics that radically departs from classical notions. Here we consider the limitations that this principle imposes due to the unpredictability of measurement outcomes of incompatible observables. For two-level systems, it is shown that any preparation violating complementarity enables the preparation of a non-signalling box violating Tsirelson's bound. Moreover, these "beyond-quantum" objects could be used to distinguish a plethora of non-orthogonal quantum states and hence enable improved cloning protocols. For higher-dimensional systems the main ideas are sketched.

QUANTUM INFORMATION PROCESSING 19[10], 358, 2020. DOI: 10.1007/s11128-020-02869-1

[P320-2020] "Long-baseline neutrino oscillation physics potential of the DUNE experiment: DUNE Collaboration"

Abi, B.; Acciarri, R.; Acero, M. A.; **Holanda, P. C. de*; Gelli, B.*; Guzzo, M. M.*; Kemp, E.*; Machado, A. A.*; Peres, O. L. G.*; Prakash, S.*; Reggiani-Guzzo, M.*; Segreto, E.*; Nunes, M. Soares*; Forero, D. V.*; Souza, H. V. de*;** et. al.

The sensitivity of the Deep Underground Neutrino Experiment (DUNE) to neutrino oscillation is determined, based on a full simulation, reconstruction, and event selection of the far detector and a full simulation and parameterized analysis of the near detector. Detailed uncertainties due to the flux prediction, neutrino interaction model, and detector effects are included. DUNE will resolve the neutrino mass ordering to a precision of 5 sigma, for all delta CP values, after 2 years of running with the nominal detector design and beam configuration. It has the potential to observe charge--parity violation in the neutrino sector to a precision of 3 sigma (5 sigma) after an exposure of 5 (10) years, for 50% of all delta CP values. It will also make precise measurements of other parameters governing long-baseline neutrino oscillation, and after an exposure of 15 years will achieve a similar sensitivity to sin22 theta 13 to current reactor experiments.

EUROPEAN PHYSICAL JOURNAL C 80[10], 978, 2020. DOI: 10.1140/epjc/s10052-020-08456-z

[P321-2020] "Machine learning applied to multifrequency data in astrophysics: blazar classification"

Arsioli, B.*; Dedin, P.*

The study of machine learning (ML) techniques for the autonomous classification of astrophysical sources is of great interest, and we explore its applications in the context of a multifrequency data-frame. We test the use of supervised ML to classify blazars according to its synchrotron peak frequency, either lower or higher than 10(15) Hz. We select a sample with 4178 blazars labelled as 1279 high synchrotron peak (HSP: nu-peak > 10(15) Hz) and 2899 low synchrotron peak (LSP: nu-peak < 10(15) Hz). A set of multifrequency features were defined to represent each source that includes spectral slopes (alpha(nu 1,nu 2)) between the radio, infra-red, optical, and X-ray bands, also considering IR colours. We describe the optimization of five ML classification algorithms that classify blazars into LSP or HSP: Random forests (RFs), support vector machine (SVM), K-nearest neighbours (KNN), Gaussian Naive Bayes (GNB), and the Ludwig auto-ML framework. In our particular case, the SVM algorithm had the best performance, reaching 93 per cent of balanced accuracy. A joint-feature permutation test revealed that the spectral slopes alpha-radio-infrared (IR) and alpha-radio-optical are the most relevant for the ML modelling, followed by the IR colours. This work shows that ML algorithms can distinguish multifrequency spectral characteristics and handle the classification of blazars into LSPs and HSPs. It is a hint for the potential use of ML for the autonomous determination of broadband spectral parameters (as the synchrotron nu-peak), or even to search for new blazars in all-sky data bases.

MONTHLY NOTICES OF THE ROYAL ASTRONOMICAL SOCIETY 498[2], 1750-1764, 2020. DOI: 10.1093/mnras/staa2449

[P322-2020] "Magnetic mesoporous silica nanospheres with dual probe & release fluorescent functionality"

Tancredi, P.; Rivas-Rojas, P. C.; Veiga, L. S.; Garate, O.; Socolovsky, L. M.; **Muraca, D.***; Ybarra, G.

The combination of different nanomaterials through step--by-step synthesis procedures has turned into a promising alternative to fabricate high-quality nanosystems in order to satisfy the increasingly demanding requirements of the biomedical field. In this work, we report a detailed study on the synthesis and characterization of a complex nanosystem composed of nanoparticles with a single magnetic nanoparticle core and a shell of dense and mesoporous silica arranged in layers. The procedure designed to fabricate these systems lead us to the formation of a dispersion of non-agglomerated spherical nanoparticles of nearly 100 nm.

The structural characterization performed over the final samples confirmed both the prevalence of single-core systems and the presence of the mesoporous silica shell in the outer layer. The performance of the nanosystem in a specific technological application was tested by sequentially loading two different fluorescents molecules by covalent and non-covalent bonding strategies. Due to the distinct loading strategies, the resulting nanosystem presented a magnetically-assisted probe & release functionality as analyzed in a magnetophoretic experiment.

NANOTECHNOLOGY 31[49], 495603, 2020. DOI: 10.1088/1361-6528/abb2c1

[P323-2020] "Measurement of B-c(2S)(+) and B-c*(2S)(+) cross section ratios in proton-proton collisions at root s=13 TeV"

Sirunyan, A. M.; Tumasyan, A.; Adam, W.; **Chinellato, J. A.*; Tonelli Manganote, E. J.*;** et. al.; CMS Collaboration

The ratios of the B-c (2S)(+) to B-c(+), B-c(*)(2S)(+) to B-c(+), and Bc(2S)(+) to Bco2STHORNthorn production cross sections are measured in proton-proton collisions at root s = 13 TeV, using a data sample collected by the CMS experiment at the LHC, corresponding to an integrated luminosity of 143 fb(-1). The three measurements are made in the Bthornc meson phase space region defined by the transverse momentum p(T) > 15 GeV and absolute rapidity vertical bar y vertical bar < 2.4, with the excited B-c((+)) (2S)(+) states reconstructed through the B-(c)(+) p thornp-, followed by the Bthornc. J=.pthorn and J=.. mu thorn mu- decays. The Bc o2STHORNthorn to Bthornc, B-c(+) (2S)(+) to Bthornc, and B-c((+)) (2S)(+) to B-c((+)) (2S)(+) cross section ratios, including the unknown B-c(+) (2S)(+). Bc ->((+)) pthorn p- branching fractions, are o3.47 +/- 0.63(stat) +/- 0.33o(syst))%, (4.69 +/- 0.71)(stat)(+) +/- 0.56(syst))%, and 1.35 +/- 0.32((stat)) +/- 0.09((syst)), respectively. None of these ratios shows a significant dependence on the pT or jyj of the B-c(+) meson. The normalized dipion invariant mass distributions from the decays B-c((*))(2S)+ -> B-c((*))pi(+)pi(-) are also reported.

PHYSICAL REVIEW D 102[9], 092007, 2020. DOI: 10.1103/PhysRevD.102.092007

[P324-2020] "Measurement of CKM matrix elements in single top quark t-channel production in proton-proton collisions at root s=13 TeV"

Sirunyan, A. M.; Tumasyan, A.; Adam, W.; **Chinellato, J. A.*; Tonelli Manganote, E. J.***; et. al.; CMS Collaboration

The first direct, model-independent measurement is presented of the modulus of the Cabibbo-Kobayashi-Maskawa (CKM) matrix elements vertical bar V-tb vertical bar, vertical bar V-td vertical bar, and vertical bar V-ts vertical bar, in final states enriched in single top quark t-channel events. The analysis uses proton-proton collision data from the LHC, collected during 2016 by the CMS experiment, at a centre--of-mass energy of 13 TeV, corresponding to an integrated luminosity of 35.9 fb(-1). Processes directly sensitive to these matrix elements are considered at both the production and decay vertices of the top quark. In the standard model hypothesis of CKM unitarity, a lower limit of vertical bar V-tb vertical bar > 0.970 is measured at the 95% confidence level. Several theories beyond the standard model are considered, and by releasing all constraints among the involved parameters, the values vertical bar V-tb vertical bar = 0.988 +/- 0.024, and vertical bar V-td vertical bar(2) + vertical bar V-ts vertical bar(2) = 0.06 +/- 0.06, where the uncertainties include both statistical and systematic components, are measured.

PHYSICS LETTERS B 808, 135609, 2020. DOI: 10.1016/j.physletb.2020.135609

[P325-2020] "Measurement of electroweak production of a W boson in avssociation with two jets in proton-proton collisions at root s=13 TeV"

Sirunyan, A. M.; Tumasyan, A.; Adam, W.; **Chinellato, J. A.*; Tonelli Manganote, E. J.***; et. al.; CMS Collaboration

A measurement is presented of electroweak (EW) production of a W boson in association with two jets in proton-proton collisions at root s = 13 TeV. The data sample was recorded by the CMS Collaboration at the LHC and corresponds to an integrated luminosity of 35.9 fb(-1). The measurement is performed for the l nu jj final state (with l nu. indicating a lepton-neutrino pair, and j representing the quarks produced in the hard interaction) in a kinematic region defined by invariant mass m(jj) > 120 GeV and transverse momenta p(Tj) > 25 GeV. The cross section of the process is measured in the electron and muon channels yielding sigma(EW)(Wjj) = 6.23 +/- 0.12 (stat)+/- 0.61 (syst) pb per channel, in agreement with leading-order standard model predictions. The additional hadronic activity of events in a signal-enriched region is studied, and the measurements are compared with predictions. The final state is also used to perform a search for anomalous trilinear gauge couplings. Limits on anomalous trilinear gauge couplings associated with dimension-six operators are given in the framework of an effective field theory. The corresponding 95% confidence level intervals are -2.3 < c(WWW)/Lambda(2) < 2.5 TeV-2, -8.8 < cW/Lambda(2) < 16 TeV-2, and -45 < c(B)/Lambda(2) < 46 TeV-2. These results are combined with the CMS EW Z(jj) analysis, yielding the constraint on the cWWW coupling: -1.8 < c(WWW)/Lambda(2) < 2.0TeV(-2).

EUROPEAN PHYSICAL JOURNAL C 80[1], 43, 2020. DOI: 10.1140/epjc/s10052-019-7585-7

[P326-2020] "Measurement of isolated photon-hadron correlations in root S-NN=5.02 TeV pp and p-Pb collisions"

Acharya, S.; Adamova, D.; Adler, A.; **Albuquerque, D. S. D.*; Chinellato, D. D.*; Takahashi, J.***; et. al.; ALICE Collaboration

This paper presents isolated photon-hadron correlations using pp and p-Pb data collected by the ALICE detector at the LHC. For photons with vertical bar eta vertical bar < 0.67 and 12 < p(T) < 40 GeV/c, the associated yield of charged particles in the range vertical bar eta vertical bar < 0.80 and 0.5 < p(T) < 10 GeV/c is presented. These momenta are much lower than previous measurements at the LHC. No significant difference between pp and p-Pb is observed, with PYTHIA 8.2 describing both data sets within uncertainties. This measurement constrains nuclear effects on the parton fragmentation in p-Pb collisions, and provides a benchmark for future studies of Pb-Pb collisions.

PHYSICAL REVIEW C 102[4], 044908, 2020. DOI: 10.1103/PhysRevC.102.044908

[P327-2020] "Measurement of t(t)over-bar normalised multi-differential cross sections in pp collisions at root s=13 TeV, and simultaneous determination of the strong coupling strength, top quark pole mass, and parton distribution functions"

Sirunyan, A. M.; Tumasyan, A.; Adam, W.; **Chinellato, J. A.*; Tonelli Manganote, E. J.***; et. al.; CMS Collaboration

Normalised multi-differential cross sections for top quark pair (t (t) over bar) production are measured in proton--proton collisions at a centre-of-mass energy of 13 TeV using events containing two oppositely charged leptons. The analysed data were recorded with the CMS detector in 2016 and correspond to an integrated luminosity of 35.9 fb(-1).

The doubledifferential t (t) over bar cross section is measured as a function of the kinematic properties of the top quark and of the t (t) over bar system at parton level in the full phase space. A triple-differential measurement is performed as a function of the invariant mass and rapidity of the t (t) over bar system and the multiplicity of additional jets at particle level. The data are compared to predictions of Monte Carlo event generators that complement next-to-leading-order (NLO) quantum chromodynamics (QCD) calculations with parton showers. Together with a fixed-order NLO QCD calculation, the triple-differential measurement is used to extract values of the strong coupling strength alpha(S) and the top quark pole mass (m(t)(pole)) using several sets of parton distribution functions (PDFs). The measurement of m(t)(pole) exploits the sensitivity of the t (t) over bar invariant mass distribution to m(t)(pole) near the production threshold. Further-more, a simultaneous fit of the PDFs, aS, and m(t)(pole) is performed at NLO, demonstrating that the new data have significant impact on the gluon PDF, and at the same time allow an accurate determination of alpha(S) and m(t)(pole). The values alpha S(mZ) = 0.1135+0.0021-0.0017 and m(t)(pole) = 170.5 +/- 0.8GeV are extracted, which account for experimental and theoretical uncertainties, the latter being estimated from NLO scale variations. Possible effects from Coulomb and soft-gluon resummation near the t (t) over bar production threshold are neglected in these parameter extractions. A rough estimate of these effects indicates an expected correction of m(t)(pole) of the order of +1 GeV, which can be regarded as additional theoretical uncertainty in the current m(t)(pole) extraction.

EUROPEAN PHYSICAL JOURNAL C 80[7], 658, 2020. DOI: 10.1140/epjc/s10052-020-7917-7

[P328-2020] "Measurement of the Low-Energy Antideuteron Inelastic Cross Section"

Acharya, S.; Adamova, D.; Adler, A.; **Albuquerque, D. S. D.*; Chinellato, D. D.*; Takahashi, J.***; et. al.; Large Ion Collider Expt Collaborat

In this Letter, we report the first measurement of the inelastic cross section for antideuteron-nucleus interactions at low particle momenta, covering a range of 0.3 <= p < 4 GeV/c. The measurement is carried out using p-Pb collisions at a center--of-mass energy per nucleon-nucleon pair of root s(NN) = 5.02 TeV, recorded with the ALICE detector at the CERN LHC and utilizing the detector material as an absorber for antideuterons and antiprotons. The extracted raw primary antiparticle--to-particle ratios are compared to the results from detailed ALICE simulations based on the GEANT4 toolkit for the propagation of (anti)particles through the detector material. The analysis of the raw primary (anti)proton spectra serves as a benchmark for this study, since their hadronic interaction cross sections are well constrained experimentally. The first measurement of the inelastic cross section for antideuteron-nucleus interactions averaged over the ALICE detector material with atomic mass numbers < A > = 17.4 and 31.8 is obtained. The measured inelastic cross section points to a possible excess with respect to the Glauber model parametrization used in GEANT4 in the lowest momentum interval of 0.3 <= p < 0.47 GeV/c up to a factor 2.1. This result is relevant for the understanding of antimatter propagation and the contributions to antinuclei production from cosmic ray interactions within the interstellar medium. In addition, the momentum range covered by this measurement is of particular importance to evaluate signal predictions for indirect dark-matter searches.

PHYSICAL REVIEW LETTERS 125[16], 162001, 2020. DOI: 10.1103/PhysRevLett.125.162001

[P329-2020] "Measurement of the Y(1S) pair production cross section and search for resonances decaying to Y(1S) mu(+)mu(-) in proton-proton collisions at root s=13 TeV"

Sirunyan, A. M.; Tumasyan, A.; Adam, W.; **Chinellato, J. A.*; Tonelli Manganote, E. J.***; et. al.; CMS Collaboration

The fiducial cross section for Y(1S) pair production in proton--proton collisions at a center-of-mass energy of 13TeVin the region where both Y(1S) mesons have an absolute rapidity below 2.0 is measured to be 79 +/- 11 (stat) +/- 6 (syst) +/- 3 (B) pbassuming the mesons are produced unpolarized. The last uncertainty corresponds to the uncertainty in the Y(1S) meson dimuon branching fraction. The measurement is performed in the final state with four muons using proton-proton collision data collected in 2016 by the CMS experiment at the LHC, corresponding to an integrated luminosity of 35.9 fb(-1). This process serves as a standard model reference in a search for narrow resonances decaying to Y(1S)mu(+)mu(-) in the same final state. Such a resonance could indicate the existence of a tetraquark that is a bound state of two bquarks and two (b) over bar antiquarks. The tetraquark search is performed for masses in the vicinity of four times the bottom quark mass, between 17.5 and 19.5 GeV, while a generic search for other resonances is performed for masses between 16.5 and 27 GeV. No significant excess of events compatible with a narrow resonance is observed in the data. Limits on the production cross section times branching fraction to four muons via an intermediate Y(1S) resonance are set as a function of the resonance mass.

PHYSICS LETTERS B 808, 135578, 2020. DOI: 10.1016/j.physletb.2020.135578

[P330-2020] "Measurements of production cross sections of WZ and same-sign WW boson pairs in association with two jets in proton-proton collisions at root s=13 TeV"

Sirunyan, A. M.; Tumasyan, A.; Adam, W.; **Chinellato, J. A.*; Tonelli Manganote, E. J.***; et. al.; CMS Collaboration

Measurements of production cross sections of WZ and same-sign WW boson pairs in association with two jets in proton-proton collisions at root s = 13 TeV at the LHC are reported. The data sample corresponds to an integrated luminosity of 137fb(-1), collected with the CMS detector during 2016-2018. The measurements are performed in the leptonic decay modes W(+/-) Z -> l(+/-)nu l'(+/-)l'(-/+) and (WW +/-)-W-+/- -> l(+/-)nu l'(+/-) nu, where l, l' = e, mu. Differential fiducial cross sections as functions of the invariant masses of the jet and charged lepton pairs, as well as of the leading-lepton transverse momentum, are measured for (WW +/-)-W-+/- production and are consistent with the standard model predictions. The dependence of differential cross sections on the invariant mass of the jet pair is also measured for WZ production. An observation of electroweak production of WZ boson pairs is reported with an observed (expected) significance of 6.8 (5.3) standard deviations. Constraints are obtained on the structure of quartic vector boson interactions in the framework of effective field theory.

PHYSICS LETTERS B 809, 135710, 2020. DOI: 10.1016/j.physletb.2020.135710

[P331-2020] "Modelling the Milky Way - I. Method and first results fitting the thick disc and halo with DES-Y3 data"

Pieres, A.; Girardi, L.; Balbinot, E.; **Sobreira, F.***; et. al.

We present a technique to fit the stellar components of the Galaxy by comparing Hess Diagrams (HDs) generated from TRILEGAL models to real data. We apply this technique, which we call MWFITTING, to photometric data from the first 3 yr of the Dark Energy Survey (DES). After removing regions containing known resolved stellar systems such as globular clusters, dwarf galaxies, nearby galaxies, the Large Magellanic Cloud, and the Sagittarius Stream, our main sample spans a total area of similar to 2300 deg(2).

We further explore a smaller subset (similar to 1300 deg(2)) that excludes all regions with known stellar streams and stellar overdensities. Validation tests on synthetic data possessing similar properties to the DES data show that the method is able to recover input parameters with a precision better than 3 per cent. We fit the DES data with an exponential thick disc model and an oblate double power-law halo model. We find that the best-fitting thick disc model has radial and vertical scale heights of 2.67 +/- 0.09 kpc and 925 +/- 40 pc, respectively. The stellar halo is fit with a broken power-law density profile with an oblateness of 0.75 +/- 0.01, an inner index of 1.82 +/- 0.08, an outer index of 4.14 +/- 0.05, and a break at 18.52 +/- 0.27 kpc from the Galactic centre. Several previously discovered stellar overdensities are recovered in the residual stellar density map, showing the reliability of MWFITTING in determining the Galactic components. Simulations made with the best-fitting parameters are a promising way to predict Milky Way star counts for surveys such as the LSST and Euclid.

MONTHLY NOTICES OF THE ROYAL ASTRONOMICAL SOCIETY 497[2], 1547-1562, 2020. DOI: 10.1093/mnras/staa1980

[P332-2020] "Multiplicity dependence of inclusive J/psi production at midrapidity in pp collisions at root s=13 TeV"

Acharya, S.; Adamova, D.; Adler, A.; **Albuquerque, D. S. D.*; Chinellato, D. D.*; Takahashi, J.***; et. al.; ALICE Collaboration

Measurements of the inclusive J/psi yield as a function of charged-particle pseudorapidity density dN(ch)/d eta in pp collisions at root s = 13 TeV with ALICE at the LHC are reported. The J/psi meson yield is measured at midrapidity (vertical bar y vertical bar < 0.9) in the dielectron channel, for events selected based on the charged-particle multiplicity at midrapidity (vertical bar eta vertical bar < 1) and at forward rapidity (-3.7 < eta < -1.7 and 2.8 < eta < 5.1); both observables are normalized to their corresponding averages in minimum bias events. The increase of the normalized J/psi yield with normalized dN(ch)/d eta is significantly stronger than linear and dependent on the transverse momentum. The data are compared to theoretical predictions, which describe the observed trends well, albeit not always quantitatively.

PHYSICS LETTERS B 810, 13575, 2020. DOI: 10.1016/j.physletb.2020.135758

[P333-2020] "Multiplicity dependence of K*(892)(0) and phi(1020) production in pp collisions at root s=13 TeV"

Acharya, S.; Adamova, D.; Adler, A.; **Albuquerque, D. S. D.*; Chinellato, D. D.*; Takahashi, J.***; et. al.; ALICE Collaboration

The striking similarities that have been observed between high-multiplicity proton-proton (pp) collisions and heavy-ion collisions can be explored through multiplicity-differential measurements of identified hadrons in pp collisions. With these measurements, it is possible to study mechanisms such as collective flow that determine the shapes of hadron transverse momentum (p(T)) spectra, to search for possible modifications of the yields of short-lived hadronic resonances due to scattering effects in an extended hadron-gas phase, and to investigate different explanations provided by phenomenological models for enhancement of strangeness production with increasing multiplicity. In this paper, these topics are addressed through measurements of the K* (892)(0) and phi(1020) mesons at midrapidity in pp collisions at root s = 13 TeV as a function of the charged-particle multiplicity. The results include the p(T) spectra, p(T)-integrated yields, mean transverse momenta, and the ratios of the yields of these resonances to those of longer-lived hadrons. Comparisons with results from other collision systems and energies, as well as predictions from phenomenological models, are also discussed.

PHYSICS LETTERS B 807, 135501, 2020. DOI: 10.1016/j.physletb.2020.135501

[P334-2020] "Neutrino interaction classification with a convolutional neural network in the DUNE far detector"

Abi, B.; Acciarri, R.; Acero, M. A.; **Holanda, P. C. de*; Gelli, B.*; Guzzo, M. M.*; Kemp, E.*; Machado, A. A.*; Peres, O. L. G.*; Prakash, S.*; Reggiani-Guzzo, M.*; Segreto, E.*; Soares Nunes, M.*; Forero, D. V.*; Souza, H. V. de***; et. al.; DUNE Collaboration

The Deep Underground Neutrino Experiment is a next-generation neutrino oscillation experiment that aims to measure CP-violation in the neutrino sector as part of a wider physics program. A deep learning approach based on a convolutional neural network has been developed to provide highly efficient and pure selections of electron neutrino and muon neutrino charged-current interactions. The electron neutrino (antineutrino) selection efficiency peaks at 90% (94%) and exceeds 85% (90%) for reconstructed neutrino energies between 2-5 GeV. The muon neutrino (antineutrino) event selection is found to have a maximum efficiency of 96% (97%) and exceeds 90% (95%) efficiency for reconstructed neutrino energies above 2 GeV. When considering all electron neutrino and antineutrino interactions as signal, a selection purity of 90% is achieved. These event selections are critical to maximize the sensitivity of the experiment to CP-violating effects.

PHYSICAL REVIEW D 102[9], 092003, 2020. DOI: 10.1103/PhysRevD.102.092003

[P335-2020] "New opportunities at the next-generation neutrino experiments I: BSM neutrino physics and dark matter"

Arguelles, C. A.; Aurisano, A. J.; Batell, B.; **Forero, D. V.*; Prakash, S.***; et al.

The combination of the high intensity proton beam facilities and massive detectors for precision measurements of neutrino oscillation parameters including the charge-parity violating (CPV) phase will open the door to help make beyond the standard model (BSM) physics reachable even in low energy regimes in the accelerator-based experiments. Large-mass detectors with highly precise tracking and energy measurements, excellent timing resolution, and low energy thresholds will enable the searches for BSM phenomena from cosmogenic origin, as well. Therefore, it is also conceivable that BSM topics in the next-generation neutrino experiments could be the dominant physics topics in the foreseeable future, as the precision of the neutrino oscillation parameter and CPV measurements continue to improve.This paper provides a review of the current landscape of BSM theory in neutrino experiments in two selected areas of the BSM topics-dark matter and neutrino related BSM-and summarizes the current results from existing neutrino experiments to set benchmarks for both theory and experiment. This paper then provides a review of upcoming neutrino experiments throughout the next 10 to 15 year time scale and their capabilities to set the foundation for potential reach in BSM physics in the two aforementioned themes. An important outcome of this paper is to ensure theoretical and simulation tools exist to carry out studies of these new areas of physics, from the first day of the experiments, such as Deep Underground Neutrino Experiment in the U.S. and Hyper-Kamiokande Experiment in Japan.

REPORTS ON PROGRESS IN PHYSICS 83[12], 124201, 2020. DOI: 10.1088/1361-6633/ab9d12

[P336-2020] "Novel sum rules for the three-point sector of QCD"

Aguilar, A. C.*; Ferreira, M. N.*; Papavassiliou, J.

For special kinematic configurations involving a single momentum scale, certain standard relations, originating from the Slavnov-Taylor identities of the theory, may be interpreted as ordinary differential equations for the "kinetic term" of the gluon propagator. The exact solutions of these equations exhibit poles at the origin, which are incompatible with the physical answer, known to diverge only logarithmically; their elimination hinges on the validity of two integral conditions that we denominate "asymmetric" and "symmetric" sum rules, depending on the kinematics employed in their derivation. The corresponding integrands contain components of the three-gluon vertex and the ghost-gluon kernel, whose dynamics are constrained when the sum rules are imposed. For the numerical treatment we single out the asymmetric sum rule, given that its support stems predominantly from low and intermediate energy regimes of the defining integral, which are physically more interesting. Adopting a combined approach based on Schwinger-Dyson equations and lattice simulations, we demonstrate how the sum rule clearly favors the suppression of an effective form factor entering in the definition of its kernel. The results of the present work offer an additional vantage point into the rich and complex structure of the three-point sector of QCD.

EUROPEAN PHYSICAL JOURNAL C 80[9], 887, 2020. DOI: 10.1140/epjc/s10052-020-08453-2

[P337-2020] "Observation of the B-s(0) -> X(3872)phi Decay"

Sirunyan, A. M.; Tumasyan, A.; Adam, W.; **Chinellato, J. A.*; Tonelli Manganote, E. J.***; et. al.; CMS Collaboration

Using a data sample of proton-proton collisions at root s = 13 TeV, corresponding to an integrated luminosity of 140 fb(-1) collected by the CMS experiment in 2016-2018, the B-s(0) -> X(3872)phi decay is observed. Decays into J/psi pi(+)pi(-) and K+K- are used to reconstruct, respectively, the X(3872) and phi. The ratio of the product of branching fractions B[B-s(0) -> X(3872)phi]B[X(3872) -> J/psi pi(+)pi(-)] to the product B[B--s(0) ->psi(2S)phi]B[psi(2S) -> J/psi pi(+)pi(-)] is measured to be [2.21 +/- 0.29(stat) +/- 0.17(syst)]%. The ratio B[B-s(0) -> X(3872)phi]/B[B-0 -> X(3872)K-0] is found to be consistent with one, while the ratio B[B-s(0) -> X(3872)phi]/B[B+-> X(3872)K+] is two times smaller. This suggests a difference in the production dynamics of the X(3872) in B-0 and B(0) s meson decays compared to B+. The reported observation may shed new light on the nature of the X(3872) particle.

PHYSICAL REVIEW LETTERS 125[15], 152001, 2020. DOI: 10.1103/PhysRevLett.125.152001

[P338-2020] "Observation of the Production of Three Massive Gauge Bosons at root s=13 TeV"

Sirunyan, A. M.; Tumasyan, A.; Adam, W.; **Chinellato, J. A.*; Tonelli Manganote, E. J.***; et. al.; CMS Collaboration

The first observation is reported of the combined production of three massive gauge bosons (VVV with V = W, Z) in proton-proton collisions at a center-of-mass energy of 13 TeV. The analysis is based on a data sample recorded by the CMS experiment at the CERN LHC corresponding to an integrated luminosity of 137 fb(-1). The searches for individualWWW, WWZ, WZZ, and ZZZ production are performed in final states with three, four, five, and six leptons (electrons or muons), or with two same-sign leptons plus one or two jets. The observed (expected) significance of the combinedVVV production signal is 5.7 (5.9) standard deviations and the corresponding measured cross section relative to the standard model prediction is 1.02(-0.23)(+0.26). The significances of the individual WWW and WWZ production are 3.3 and 3.4 standard deviations, respectively. Measured production cross sections for the individual triboson processes are also reported.

PHYSICAL REVIEW LETTERS 125[15], 151802, 2020. DOI: 10.1103/PhysRevLett.125.151802

[P339-2020] "On the sulfur doping of gamma-graphdiyne: A Molecular Dynamics and DFT study"

Oliveira, E. F.*; Batagin Neto, A.; **Galvão, D. S.***

Recently, an experimental study developed an efficient way to obtain sulfur-doped gamma-graphdiyne. This study has shown that this new material could have promising applications in lithium-ion batteries, but the complete understanding of how the sulfur atoms are incorporated into the graphdiyne network is still missing. In this work, we have investigated the sulfur doping process through molecular dynamics and density functional theory simulations. Our results suggest that the doped induced distortions of the gamma--graphdiyne pores prevent the incorporation of more than two sulfur atoms. The most common configuration is the incorporation of just one sulfur atom per the graphdiyne pore.

MRS ADVANCES 5[52-53][SI], 2701-2706, PII S2059852120002558 2020. DOI: 10.1557/adv.2020.255

[P340-2020] "Optical follow-up of gravitational wave triggers with DECam during the first two LIGO/VIRGO observing runs"

Herner, K.; Annis, J.; Brout, D.; **Sobreira, F.***; et. al.;

Gravitational wave (GW) events detectable by LIGO and Virgo have several possible progenitors, including black hole mergers, neutron star mergers, black hole-neutron star mergers, supernovae, and cosmic string cusps. A subset of GW events is expected to produce electromagnetic (EM) emission that, once detected, will provide complementary information about their astrophysical context. To that end, the LIGO-Virgo Collaboration (LVC) sends GW candidate alerts to the astronomical community so that searches for their EM counterparts can be pursued. The DESGW group, consisting of members of the Dark Energy Survey (DES), the LVC, and other members of the astronomical community, uses the Dark Energy Camera (DECam) to perform a search and discovery program for optical signatures of LVC GW events. DESGW aims to use a sample of GW events as standard sirens for cosmology. Due to the short decay timescale of the expected EM counterparts and the need to quickly eliminate survey areas with no counterpart candidates, it is critical to complete the initial analysis of each night's images as quickly as possible. We discuss our search area determination, imaging pipeline, and candidate selection processes. We review results from the DESGW program during the first two LIGO-Virgo observing campaigns and introduce other science applications that our pipeline enables.

ASTRONOMY AND COMPUTING 33, 100425, 2020. DOI: 10.1016/j.ascom.2020.100425

[P341-2020] "Physicochemical Studies on the Surface of Polyamide 6.6 Fabrics Functionalized by DBD Plasmas Operated at Atmospheric and Sub-Atmospheric Pressures"

Nascimento, L.; Gasi, F.; **Landers, R.***; Silva Sobrinho, A. da; Aragão, E.; Fraga, M.; Petraconi, G.; Chiappim, W.; Pessoa, R.

This work proposes the use of a dielectric barrier discharge (DBD) reactor operating at atmospheric pressure (AP) using air and sub-atmospheric pressure (SAP) using air or argon to treat polyamide 6.6 (PA6.6) fabrics. Here, plasma dosages corresponding to 37.5 kW center dot min center dot m(-2)for AP and 7.5 kW center dot min center dot m(-2)for SAP in air or argon were used. The hydrophilicity aging effect property of untreated and DBD-treated PA6.6 samples was evaluated from the apparent contact angle. The surface changes in physical microstructure were studied by field emission scanning electron microscopy (FE-SEM). To prove the changes in chemical functional groups in the fibers, Fourier transform infrared spectroscopy (FTIR) was used, and the change in surface bonds was evaluated by energy dispersive X-ray spectroscopy (EDS) and X-ray photoelectron spectroscopy (XPS). In addition, the whiteness effect was investigated by the color spectrophotometry (Datacolor) technique. The results showed that the increase in surface roughness by the SAP DBD treatment contributed to a decrease in and maintenance of the hydrophilicity of PA6.6 fabrics for longer. The SAP DBD in air treatment promoted an enhancement of the aging effect with a low plasma dosage (5-fold reduction compared with AP DBD treatment). Finally, the SAP DBD treatment using argon functionalizes the fabric surface more efficiently than DBD treatments in air.

POLYMERS 12[9], 2128, 2020. DOI: 10.3390/polym12092128

[P342-2020] "Piezoelectric Actuation of Graphene-Coated Polar Structures"

Kholkin, A. L.; Ushakov, A. D.; Chuvakova, M. A.; Kosobokov, M. S.; Akhmatkhanov, A. R.; Turutin, A. V.; Chichkov, M. V.; Kravchenko, I. I.; **Kopelevich, Y.***; Shur, V. Y.

Ferroelectric materials based on lead zirconate titanate (PZT) are widely used as sensors and actuators because of their strong piezoelectric activity. However, their application is limited because of the high processing temperature, brittleness, lack of conformal deposition, and a limited possibility to be integrated with the microelectromechanical systems (MEMS). Recent studies on the piezoelectricity in the 2-D materials have demonstrated their potential in these applications, essentially due to their flexibility and integrability with the MEMS. In this work, we deposited a few layer graphene (FLG) on the amorphous oxidized Si3N4 membranes and studied their piezoelectric response by sensitive laser interferometry and rigorous finite-element modeling (FEM) analysis. Modal analysis by FEM and comparison with the experimental results show that the driving force for the piezoelectric-like response can be a polar interface layer formed between the residual oxygen in Si3N4 and the FLG. The response was about 14 nm/V at resonance and could be further enhanced by adjusting the geometry of the device. These phenomena are fully consistent with the earlier piezoresponse force microscopy (PFM) observations of the piezoelectricity of the graphene on SiO2 and open up an avenue for using graphene-coated structures in the MEMS.

IEEE TRANSACTIONS ON ULTRASONICS FERROELECTRICS AND FREQUENCY CONTROL 67[10], 2142-2147, 2020. DOI: 10.1109/TUFFC.2020.2998976

[P343-2020] "Pileup mitigation at CMS in 13 TeV data"

Sirunyan, A. M.; Tumasyan, A.; Adam, W.; **Chinellato, J. A.*; Tonelli Manganote, E. J.***; et. al.; CMS Collaboration

With increasing instantaneous luminosity at the LHC come additional reconstruction challenges. At high luminosity, many collisions occur simultaneously within one proton-proton bunch crossing. The isolation of an interesting collision from the additional "pileup" collisions is needed for effective physics performance. In the CMS Collaboration, several techniques capable of mitigating the impact of these pileup collisions have been developed. Such methods include charged-hadron subtraction, pileup jet identification, isospin-based neutral particle "delta beta" correction, and, most recently, pileup per particle identification. This paper surveys the performance of these techniques for jet and missing transverse momentum reconstruction, as well as muon isolation. The analysis makes use of data corresponding to 35.9 fb(-1) collected with the CMS experiment in 2016 at a center-of-mass energy of 13 TeV. The performance of each algorithm is discussed for up to 70 simultaneous collisions per bunch crossing. Significant improvements are found in the identification of pileup jets, the jet energy, mass, and angular resolution, missing transverse momentum resolution, and muon isolation when using pileup per particle identification.

JOURNAL OF INSTRUMENTATION 15[9], P09018, 2020. DOI: 10.1088/1748-0221/15/09/P09018

[P344-2020] "QCD challenges from pp to A-A collisions"

Adolfsson, J.; Andronic, A.; Bierlich, C.; **Chinellato, D. D.*; Silva, A. V. D.***; et al.

This paper is a write-up of the ideas that were presented, developed and discussed at the third International Workshop on QCD Challenges from pp to A-A, which took place in August 2019 in Lund, Sweden (Workshop link:). The goal of the workshop was to focus on some of the open questions in the field and try to come up with concrete suggestions for how to make progress on both the experimental and theoretical sides. The paper gives a brief introduction to each topic and then summarizes the primary results.

EUROPEAN PHYSICAL JOURNAL A 56[11], 288, 2020. DOI: 10.1140/epja/s10050-020-00270-1

[P345-2020] "Reconstruction of signal amplitudes in the CMS electromagnetic calorimeter in the presence of overlapping proton-proton interactions"

Sirunyan, A. M.; Tumasyan, A.; Adam, W.; **Chinellato, J. A.*; Tonelli Manganote, E. J.*;** et. al.; CMS Collaboration

A template fitting technique for reconstructing the amplitude of signals produced by the lead tungstate crystals of the CMS electromagnetic calorimeter is described. This novel approach is designed to suppress the contribution to the signal of the increased number of out-of-time interactions per beam crossing following the reduction of the accelerator bunch spacing from 50 to 25 ns at the start of Run 2 of the LHC. Execution of the algorithm is sufficiently fast for it to be employed in the CMS high-level trigger. It is also used in the offline event reconstruction. Results obtained from simulations and from Run 2 collision data (2015-2018) demonstrate a substantial improvement in the energy resolution of the calorimeter over a range of energies extending from a few GeV to several tens of GeV.

JOURNAL OF INSTRUMENTATION 15[10], P10002, 2020. DOI: 10.1088/1748-0221/15/10/P10002

[P346-2020] "Role of Rare Earth Elements and Entropy on the Anatase-To-Rutile Phase Transformation of TiO2 Thin Films Deposited by Ion Beam Sputtering"

Scoca, D. L. S.*; Cemin, F.*; Bilmes, S. A.; Figueroa, C. A.; Zanatta, A. R.; **Alvarez, F.***

The role played by oxygen vacancies and rare earth (RE) elements in the anatase-to-rutile (A-R) phase transformation of titanium dioxide (TiO2) is still a matter of controversy. Here, we report the A-R transformation of TiO2 thin solid films as obtained by ion beam sputtering a RE-decorated titanium target in an oxygen-rich atmosphere. The samples correspond to undoped, single-doped (Sm, Tm, and Tb), and codoped (Sm:Tb, Sm:Tm, and Sm:Tb:Tm) TiO2 films. In the as-prepared form, the films are amorphous and contain similar to 0.5 at. % of each RE. The structural modifications of the TiO2 films due to the RE elements and the annealing treatments in an oxygen atmosphere are described according to the experimental results provided by Raman scattering, X-ray photoelectron spectroscopy, and optical measurements. The A-R transformation depends on both the annealing temperature and the characteristics of the undoped, single-doped, and codoped TiO2 films. As reported in the literature, the A-R transformation can be inhibited or enhanced by the presence of impurities and is mostly related to energetic contributions. The experimental results were analyzed, considering the essential and stabilizing role of the entropy of mixing in the A-R transformation due to the introduction of more and multiple quantum states originated in vacancies and impurities in the anatase phase.

ACS OMEGA 5[43], 28027-28036, 2020. DOI: 10.1021/acsomega.0c03431

[P347-2020] "Schwarzites to schwarzynes: A new class of superdeformable materials"

Oliveira, E. F.*; Galvão, D. S.*

In this work, we have investigated the structural and mechanical properties of a new class of soft and superelastic materials, called schwarzynes. These materials are obtained by inserting sp carbon atoms (acetylenic groups) into the schwarzite framework. Using fully atomistic molecular dynamics simulations with the AIREBO force field, our results show that schwarzynes are stable materials up to high temperatures (1000K). Schwarzynes exhibit a very wide elastic regime, some of them up to 70% strain without structural fractures. Our preliminary results show that the elastic properties can be easily engineered by tuning the number of acetylenic groups and the crystallographic directions where they are inserted.

MRS ADVANCES 5[37-38][SI], 1947-1954, 2020. DOI: 10.1557/adv.2020.298

[P348-2020] "Search for a light charged Higgs boson in the H-+/- -> cs channel in proton-proton collisions at root s=13 TeV"

Sirunyan, A. M.; Tumasyan, A.; Adam, W.; **Chinellato, J. A.*; Tonelli Manganote, E. J.***; et. al.; CMS Collaboration

A search is conducted for a low-mass charged Higgs boson produced in a top quark decay and subsequently decaying into a charm and a strange quark. The data sample was recorded in proton-proton collisions at root s = 13 TeV by the CMS experiment at the LHC and corresponds to an integrated luminosity of 35.9 fb(-1). The search is performed in the process of top quark pair production, where one top quark decays to a bottom quark and a charged Higgs boson and the other to a bottom quark and a W boson. With the W boson decaying to a charged lepton (electron or muon) and a neutrino, the final state comprises an isolated lepton, missing transverse momentum, and at least four jets, of which two are tagged as b jets. To enhance the search sensitivity, one of the jets originating from the charged Higgs boson is required to satisfy a charm tagging selection. No significant excess beyond standard model predictions is found in the dijet invariant mass distribution. An upper limit in the range 1.68%-0.25% is set on the branching fraction of the top quark decay to the charged Higgs boson and bottom quark for a charged Higgs boson mass between 80 and 160 GeV.

PHYSICAL REVIEW D 102[7], 072001, 2020. DOI: 10.1103/PhysRevD.102.072001

[P349-2020] "Search for disappearing tracks in proton-proton collisions at root s=13 TeV"

Sirunyan, A. M.; Tumasyan, A.; Adam, W.; **Chinellato, J. A.*; Tonelli Manganote, E. J.***; et. al.; CMS Collaboration

A search is presented for long-lived charged particles that decay within the volume of the silicon tracker of the CMS experiment. Such particles can produce events with an isolated track that is missing hits in the outermost layers of the silicon tracker, and is also associated with little energy deposited in the calorimeters and no hits in the muon detectors. The search for events with this "disappearing track" signature is performed in a sample of proton-proton collisions recorded by the CMS experiment at the LHC with a center-of-mass energy of 13 TeV, corresponding to an integrated luminosity of 101 fb(-1) recorded in 2017 and 2018. The observation of 48 events is consistent with the estimated background of 47.8(-2.3)(+2.7) (stat) +/- 8.1 (syst) events. Upper limits are set on chargino production in the context of an anomaly-mediated supersymmetry breaking model for purely wino and higgsino neutralino scenarios. At 95% confidence level, the first constraint is placed on chargino masses in the higgsino case, excluding below 750 (175)GeV for a lifetime of 3 (0.05)ns. In the wino case, the results of this search are combined with a previous CMS search to produce a result representing the complete LHC data set recorded in 2015-2018, the most stringent constraints to date. At 95% confidence level, chargino masses in the wino case are excluded below 884 (474)GeV for a lifetime of 3 (0.2)ns.

PHYSICS LETTERS B 806, 135502, 2020. DOI: 10.1016/j.physletb.2020.135502

[P350-2020] "Search for supersymmetry in proton-proton collisions at root s=13 TeV in events with high-momentum Z bosons and missing transverse momentum"

Sirunyan, A. M.; Tumasyan, A.; Adam, W.; **Chinellato, J. A.*; Tonelli Manganote, E. J.***; et. al.; CMS Collaboration

A search for new physics in events with two highly Lorentz--boosted Z bosons and large missing transverse momentum is presented. The analyzed proton-proton collision data, corresponding to an integrated luminosity of 137 fb(-1), were recorded at s = 13 TeV by the CMS experiment at the CERN LHC. The search utilizes the substructure of jets with large radius to identify quark pairs from Z boson decays. Backgrounds from standard model processes are suppressed by requirements on the jet mass and the missing transverse momentum. No significant excess in the event yield is observed beyond the number of background events expected from the standard model. For a simplified supersymmetric model in which the Z bosons arise from the decay of gluinos, an exclusion limit of 1920 GeV on the gluino mass is set at 95% confidence level. This is the first search for beyond-standard-model production of pairs of boosted Z bosons plus large missing transverse momentum.

JOURNAL OF HIGH ENERGY PHYSICS 9, 149, 2020. DOI: 10.1007/JHEP09(2020)149

[P351-2020] "Studies on the response of a water-Cherenkov detector of the Pierre Auger Observatory to atmospheric muons using an RPC hodoscope"

Aab, A.; Abreu, P.; Aglietta, M.; **Chinellato, J. A.*; de Oliveira Franco, D.*; Castro, M. L. Diaz*; Dobrigkeit, C.*; Fauth, A. C.*; Machado Payeras, A.*; Muller, M. A.***; et. al.; Pierre Auger Collaboration

Extensive air showers, originating from ultra-high energy cosmic rays, have been successfully measured through the use of arrays of water-Cherenkov detectors (WCDs). Sophisticated analyses exploitingWCD data have made it possible to demonstrate that shower simulations, based on different hadronic-interaction models, cannot reproduce the observed number of muons at the ground. The accurate knowledge of the WCD response to muons is paramount in establishing the exact level of this discrepancy. In this work, we report on a study of the response of a WCD of the PierreAuger Observatory to atmospheric muons performed with a hodoscope made of resistive plate chambers (RPCs), enabling us to select and reconstruct nearly 600 thousand single muon trajectories with zenith angles ranging from 0 degrees to 55 degrees. Comparison of distributions of key observables between the hodoscope data and the predictions of dedicated simulations allows us to demonstrate the accuracy of the latter at a level of 2%. As the WCD calibration is based on its response to atmospheric muons, the hodoscope data are also exploited to show the long-term stability of the procedure.

JOURNAL OF INSTRUMENTATION 15[9], P09002, 2020. DOI: 10.1088/1748-0221/15/09/P09002

[P352-2020] "Synthesis of bioactive glass-based coating by plasma electrolytic oxidation: Untangling a new deposition pathway toward titanium implant surfaces"

Costa, R. C.; Souza, J. G. S.; Cordeiro, J. M.; Bertolini, M.; de Avila, E. D.; **Landers, R.***; Rangel, E. C.; Fortulan, C. A.; Retamal-Valdes, B.; da Cruz, N. C.; Feres, M.; Barao, V. A. R.

Hypothesis: Although bioactive glass (BG) particle coatings were previously developed by different methods, poor particle adhesion to surfaces and reduced biological effects because of glass crystallization have limited their biomedical applications. To overcome this problem, we have untangled, for the first time, plasma electrolytic oxidation (PEO) as a new pathway for the synthesis of bioactive glass-based coating (PEO-BG) on titanium (Ti) materials. Experiments: Electrolyte solution with bioactive elements (Na2SiO3-5H(2)O, C4H6O4Ca, NaNO3, and C3H7Na2O6P) was used as a precursor source to obtain a 45S5 bioglass-like composition on a Ti surface by PEO. Subsequently, the PEO-BG coating was investigated with respect to its surface, mechanical, tribological, electrochemical, microbiological, and biological properties, compared with those of machined and sandblasted/acid-etched control surfaces. Findings: PEO treatment produced a coating with complex surface topography, Ti crystalline phases, superhydrophilic status, chemical composition, and oxide layer similar to that of 4555-6G (similar to 45.0Si, 24.5 Ca, 24.5Na, 6.0P w/v%). PEO-BG enhanced Ti mechanical and tribological properties with higher corrosion resistance. Furthermore, PEO-BG had a positive influence in polymicrobial biofilms, by reducing pathogenic bacterial associated with biofilm-related infections. PEO-BG also showed higher adsorption of blood plasma proteins without cytotoxic effects on human cells, and thus may be considered a promising biocompatible approach for biomedical implants.

JOURNAL OF COLLOID AND INTERFACE SCIENCE 579, 680-698, 2020. DOI: 10.1016/j.jcis.2020.06.102

[P353-2020] "Tc-99m-sestamibi SPECT/CT and(18)F-FDG--PET/CT have similar performance but different imaging patterns in newly diagnosed multiple myeloma"

Mosci, C.; Pericole, F. V.; Oliveira, G. B.; Delamain, M. T.; **Takahashi, M. E. S.***; Carvalheira, J. B. C.; Etchebehere, E. C. S. C.; Santos, A. O.; Miranda, E. C. M.; Lima, M. C. L.; Amorim, B. J.; Souza, C. A. de; Lorand-Metze, I.; Ramos, C. D.

Purpose F-18-fluorodeoxiglucose (F-18-FDG)-PET/CT has been widely used to evaluate multiple myeloma.Tc-99m-sestamibi (MIBI) scintigraphy has also been proposed for assessing multiple myeloma, but its use with state-of-the-art single-photon emission computed tomography/computed tomography (SPECT/CT) technology has not been fully evaluated.This study aimed to compare these two imaging modalities in multiple myeloma staging. Materials and methods Sixty-two patients with recently diagnosed multiple myeloma were submitted to whole-body(18)F-FDG-PET/CT and whole-body MIBI scans plus SPECT/CT of the chest and abdomen/pelvis. Number of focal lesions, contiguous soft tissue involvement (CSTI), extramedullary lesions (EMLs) and diffuse bone marrow (BM) involvement were recorded. Results PET/CT was positive in 59 patients (95%) and MIBI SPECT/CT in 58 (93%) (P = 0.69). MIBI detected more diffuse bone marrow involvement than PET/CT (respectively 78 vs. 58% of the patients), while PET/CT demonstrated more focal lesions than MIBI SPECT/CT (81 vs. 54% of the patients) (P = 0.002). PET/CT detected EMLs in four subjects and MIBI in one subject. CSTI was found in 28 (45%) and 23 (37%) patients on PET/CT and MIBI images, respectively (P = 0.36). Three patients with lytic lesions and no FDG uptake were MIBI positive, and two subjects with lytic lesions without MIBI uptake were FDG positive. Conclusion MIBI SPECT/CT performs similarly to(18)F-FDG-PET/CT in identifying sites of active disease in multiple myeloma staging. MIBI is more efficient than FDG for detecting the diffuse involvement of bone marrow but less efficient for detecting focal lesions. Some patients presented a 'mismatch' pattern of FDG/MIBI uptake.

NUCLEAR MEDICINE COMMUNICATIONS 41[10], 1081-1088, 2020. DOI: 10.1097/MNM.0000000000001259

[P354-2020] "Theory of optical tweezing of dielectric microspheres in chiral host media and its applications"

Ali, R.*; Dutra, R. S.; Pinheiro, F. A.; Rosa, F. S. S.; Maia Neto, P. A.

We report for the first time the theory of optical tweezers of spherical dielectric particles embedded in a chiral medium. We develop a partial-wave (Mie) expansion to calculate the optical force acting on a dielectric microsphere illuminated by a circularly-polarized, highly focused laser beam. When choosing a polarization with the same handedness of the medium, the axial trap stability is improved, thus allowing for tweezing of high-refractive-index particles. When the particle is displaced off-axis by an external force, its equilibrium position is rotated around the optical axis by the mechanical effect of an optical torque. Both the optical torque and the angle of rotation are greatly enhanced in the presence of a chiral host medium when considering radii a few times larger than the wavelength. In this range, the angle of rotation depends strongly on the microsphere radius and the chirality parameter of the host medium, opening the way for a quantitative characterization of both parameters. Measurable angles are predicted even in the case of naturally occurring chiral solutes, allowing for a novel all-optical method to locally probe the chiral response at the nanoscale.

SCIENTIFIC REPORTS 10[1], 16481, 2020. DOI: 10.1038/s41598-020-73530-1

[P355-2020] "Thermodynamic control -An old paradigm with new applications"

Deffner, S.; **Bonança, M. V. S.***

Tremendous research efforts have been invested in exploring and designing so-called shortcuts to adiabaticity. These are finite-time processes that produce the same final states that would result from infinitely slow driving. Most of these techniques rely on auxiliary fields and quantum control, which makes them rather costly to implement. In this Perspective we outline an alternative paradigm for optimal control that has proven powerful in a wide variety of situations ranging from heat engines over chemical reactions to quantum dynamics -thermodynamic control. Focusing on only a few, selected milestones we seek to provide a pedagogical entry point into this powerful and versatile framework.

EPL 131[2], 20001, 2020. DOI: 10.1209/0295-5075/131/20001

[P356-2020] "Time-Resolved Photoluminescence in Heterostructures with InGaAs:Cr/GaAs Quantum Wells"

Dorokhin, M., V; Demina, P. B.; Danilov, Yu A.; Vikhrova, O. V.; Kuznetsov, Yu M.; Ved', M. V.; **Iikawa, F.***; Balanta, M. A. G.

The results of studies of the time-resolved photoluminescence in semiconductor heterostructures containing two noninteracting InGaAs quantum wells in a GaAs matrix are reported. One of the quantum wells was undoped, and the other was uniformly doped with chromium atoms (InGaAs:Cr). It was shown that the introduction of Cr had a profound effect on the recombination lifetime of charge carriers in quantum wells. The change in the photoluminescence intensity after excitation cannot be described by a monoexponential decay function, which is attributed to a change in the built-in electric field of the surface barrier in the quantum wells because of screening by photoexcited charge carriers.

SEMICONDUCTORS 54[10], 1341-1346, 2020. DOI: 10.1134/S1063782620100061

[P357-2020] "Tuning the crystalline electric field and magnetic anisotropy along the CeCuBi2-xSbx series"

Freitas, G. S.*; Piva, M. M.*; Grossi, R.*; Jesus, C. B. R.; **Souza, J. C.*; Christovam, D. S.***; Oliveira, N. F.; Leao, J. B.; **Adriano, C.***; Lynn, J. W.; **Pagliuso, P. G.***

We have performed x-ray powder diffraction, magnetization, electrical resistivity, heat capacity, and inelastic neutron scattering (INS) to investigate the physical properties of the intermetallic series of compounds, CeCuBi2-xSbx. These compounds crystallize in a tetragonal structure with space group P4/nmm and present antiferromagnetic transition temperatures ranging from 3.6 to 16 K. Remarkably, the magnetization easy axis changes along the series, which is closely related to the variations of the tetragonal crystalline electric-field (CEF) parameters. This evolution was analyzed using a mean-field model, which included anisotropic nearest-neighbor interactions and the tetragonal CEF Hamiltonian. The CEF parameters were obtained by fitting the magnetic susceptibility data with the constraints given by the INS measurements. Finally, we discuss how this CEF evolution can affect the Kondo physics and the search for a superconducting state in this family.

PHYSICAL REVIEW B 102[15], 155129, 2020. DOI: 10.1103/PhysRevB.102.155129

[P358-2020] "Ultra-fast kinematic vortices in mesoscopic superconductors: the effect of the self-field"

Cadorim, L. R.; **Oliveira Junior, A. de***; Sardella, E.

Within the framework of the generalized time-dependent Ginzburg-Landau equations, we studied the influence of the magnetic self-field induced by the currents inside a superconducting sample driven by an applied transport current. The numerical simulations of the resistive state of the system show that neither material inhomogeneity nor a normal contact smaller than the sample width are required to produce an inhomogeneous current distribution inside the sample, which leads to the emergence of a kinematic vortex-antivortex pair (vortex street) solution. Further, we discuss the behaviors of the kinematic vortex velocity, the annihilation rates of the supercurrent, and the superconducting order parameters alongside the vortex street solution. We prove that these two latter points explain the characteristics of the resistive state of the system. They are the fundamental basis to describe the peak of the current-resistance characteristic curve and the location where the vortex-antivortex pair is formed.

SCIENTIFIC REPORTS 10[1], 18662, 2020. DOI: 10.1038/s41598-020-75748-5

[P359-2020] "Unconventional enhancement of ferromagnetic interactions in Cd-doped GdFe2Zn20 single crystals studied by ESR and Fe-57 Mossbauer spectroscopies"

Cabrera-Baez, M.; Munevar, J.; Couto-Mota, R. M.; Camejo, Y. M.; Contreras, C.; Baggio-Saitovitch, E.; Avila, M. A.; **Rettori, C.***

Single crystals of GdFe2Zn20-xCdx ($0.0 < x < 1.4$) were grown and characterized through structural, magnetic, and electronic properties using x-ray diffraction, field- and temperature--dependent magnetization, specific heat, 57 Fe Mossbauer spectroscopy, and electron spin resonance (ESR). A negative chemical pressure effect is accompanied by an unexpected increase of T-C from 86 to 96 K, together with a reduction of the magnetic effective moment and saturation magnetic moment, as evidenced by all of the experimental techniques. From the microscopic point of view, probing at the 4f electron level and the Fe nucleus has allowed the extraction of important information about the configuration and the effective role of the partial Cd substitution for Zn in this ferromagnetic system. Our Fe-57 Mossbauer spectroscopy experiments show a negligible variation of the hyperfine field at the Fe site, and ESR experiments reveal an enhancement of the Korringa-type relaxation and a molecular field effect as Cd is incorporated. This complex behavior is assigned to a possible reconstruction of the Fermi surface and/or a new distribution of the d type of conduction electrons in response to the negative chemical pressure, leading to an enhancement of the ferromagnetic transition temperature in a generalized Ruderman-Kittel-Kasuya-Yosida interaction scenario.

PHYSICAL REVIEW B 102[14], 144420, 2020. DOI: 10.1103/PhysRevB.102.144420

[P360-2020] "Unit cell volume reduction of Gd5(Si,Ge)4 nanoparticles controlled by bulk compressibility"

Andrade, V. M.*; Belo, J. H.; Checca, N. R.; Rossi, A.; Garcia, F.; Almeida, B.; Tedesco, J. C. G.; Poulain, A.; Pereira, A. M.; Reis, M. S.; Araujo, J. P.

The production of Gd-5(Si,Ge)(4) compounds in reduced dimensionality, through pulsed laser deposition (PLD), have shown their potential for practical applications. Here, we present nanoparticles ranging from 10 to 27 nm of average particle size of Gd-5(SixGe1-x)(4), with x = 0, 0.45 and 0.60, obtained using an Nd:Yag (1064 nm) and an Excimer KrF laser (248 nm). Synchrotron X-ray Diffraction measurements revealed a reduced unit cell volume in comparison to their bulk counterpart.

The x = 0 sample presented a similar to 1.99% reduction while x = 0.45 composition, a shrinkage of similar to 1.81% on the unit cell volume that are a result of a structural change to a Gd5Si4-type structure [O(I)]. In contrast, x = 0.60 nanoparticles conserve the bulk crystal structure with similar to 0.95% of volume shrinkage. As a consequence, there is a change on the magnetic transition order from a first to a second one for all nanostructures followed by a magnetocaloric response reduction. These observations unveil a direct correlation between the bulk compressibility values and the unit cell shrinkage, suggesting that the rise of a surface stress plays a major role on the particle and unit cell dimensions.

JOURNAL OF ALLOYS AND COMPOUNDS 849, 156384, 2020. DOI: 10.1016/j.jallcom.2020.156384

[P361-2020] "Upsilon production in p-Pb collisions at root s(NN)=8.16 TeV"

Acharya, S.; Adamova, D.; Adler, A.; **Albuquerque, D. S. D.*; Chinellato, D. D.*; Takahashi, J.***; et. al.; ALICE Collaboration

Upsilon production in p-Pb interactions is studied at the centre-of-mass energy per nucleon-nucleon collision root s = 8.16 TeV with the ALICE detector at the CERN LHC. The measurement is performed reconstructing bottomonium resonances via their dimuon decay channel, in the centre-of-mass rapidity intervals 2.03 < 3.53 and -4.46 y -2.96, down to zero transverse momentum. In this work, results on the Upsilon(1S) production cross section as a function of rapidity and transverse momentum are presented. The corresponding nuclear modification factor shows a suppression of the Upsilon(1S) yields with respect to pp collisions, both at forward and backward rapidity. This suppression is stronger in the low transverse momentum region and shows no significant dependence on the centrality of the interactions. Furthermore, the Upsilon(2S) nuclear modification factor is evaluated, suggesting a suppression similar to that of the Upsilon(1S). A first measurement of the Upsilon(3S) has also been performed. Finally, results are compared with previous ALICE measurements in p-Pb collisions at root s= 5.02 TeV and with theoretical calculations.

PHYSICS LETTERS B 806, 135486, 2020. DOI: 10.1016/j.physletb.2020.135486

[P362-2020] "Using black carbon modified with NbMo and NbPd oxide nanoparticles for the improvement of H2O2 electrosynthesis"

Trevelin, L. C.; **Valim, R. B.***; Carneiro, J. F.; **Siervo, A. de***; Rocha, R. S.; Lanza, M. R., V.

Oxygen reduction reaction (ORR) is an important reaction with applications in advanced oxidative processes through in aim hydrogen peroxide electrogeneration. Oxygen can be reduced either to hydrogen peroxide via two-electron pathway or in a competitive way to water via four-electron pathway. This study shows the application of Printex L6 carbon modified with niobium/molybdenum or niobium/palladium oxides for H2O2 generation in K2SO4 0.1 mol L-1 (pH 2), where the modified carbon contributed to an increase in electroconductivity compared to unmodified carbon. The catalysts were prepared by the polymeric precursor method and were analyzed by x-ray absorption near edge structure (XANES), x-ray diffraction (XRD), and xray photoelectron spectroscopy (XPS) which showed the presence of orthorhombic Nb2O5 and MoO3 and tetragonal PdO independent phases. Also, the data obtained from x-ray fluorescence (FRX) and transmission electron microscopy (TEM) showed particle size of about 5 nm for the modified Printex L6 carbon compared to 25-30 nm for the unmodified Printex L6 carbon in an almost homogeneous distribution on the carbon surface. Based on the electrochemical analyses, the values obtained for H2O2 selectivity were 77, 77 and 88% for 5% Nb50Mo50/C, 5%Nb90Pd10/C, and 5% Nb95Pd05/C, respectively, compared to 89% for unmodified Printex L6 carbon. The materials investigated presented potential shifts of 110, 420 and 340 mV for 5% Nb50Mo50/C, 5%Nb-90Pd-10/C and 5%Nb95Pd05/C, respectively, compared to Printex L6 carbon at a determined current density.

JOURNAL OF ELECTROANALYTICAL CHEMISTRY 877, 114746, 2020. DOI: 10.1016/j.jelechem.2020.114746

[P363-2020] "W+ W- boson pair production in proton-proton collisions at root s=13 TeV"

Sirunyan, A. M.; Tumasyan, A.; Adam, W.; **Chinellato, J. A.*; Tonelli Manganote, E. J.***; et. al.; CMS Collaboration

A measurement of the W+W- boson pair production cross section in proton-proton collisions at root s = 13 TeV is presented. The data used in this study are collected with the CMS detector at the CERN LHC and correspond to an integrated luminosity of 35.9 fb(-1). The W+W- candidate events are selected by requiring two oppositely charged leptons (electrons or muons). Two methods for reducing background contributions are employed. In the first one, a sequence of requirements on kinematic quantities is applied allowing a measurement of the total production cross section, 117.6 +/- 6.8 pb, which agrees well with the theoretical prediction. Fiducial cross sections are also reported for events with zero or one jet, and the change in the zero-jet fiducial cross section with the jet transverse momentum threshold is measured. Normalized differential cross sections are reported within the fiducial region. A second method for suppressing background contributions employs two random forest classifiers. The analysis based on this method includes a measurement of the total production cross section and also a measurement of the normalized jet multiplicity distribution in W+W- events. Finally, a dilepton invariant mass distribution is used to probe for physics beyond the standard model in the context of an effective field theory, and constraints on the presence of dimension-6 operators are derived.

PHYSICAL REVIEW D 102[9], 092001, 2020. DOI: 10.1103/PhysRevD.102.092001

[P364-2020] "Z-boson production in p-Pb collisions at root s(NN) =8.16 TeV and Pb-Pb collisions at root s(NN) =5.02 TeV"

Acharya, S.; Adamova, D.; Adler, A.; **Albuquerque, D. S. D.*; Chinellato, D. D.*; Takahashi, J.***; et. al.; ALICE Collaboration

Measurement of Z-boson production in p-Pb collisions at 8.16 TeV and Pb-Pb collisions at = 5.02 TeV is reported. It is performed in the dimuon decay channel, through the detection of muons with pseudorapidity -4 < <eta>(mu)< -2.5 and transverse momentum pT<mu>> 20 GeV/c in the laboratory frame. The invariant yield and nuclear modification factor are measured for opposite-sign dimuons with invariant mass 60 < m(<mu>mu)< 120 GeV/c(2) and rapidity 2.5 <ycms mu mu< 4. They are presented as a function of rapidity and, for the Pb-Pb collisions, of centrality as well. The results are compared with theoretical calculations, both with and without nuclear modifications to the Parton Distribution Functions (PDFs). In p-Pb collisions the center-of-mass frame is boosted with respect to the laboratory frame, and the measurements cover the backward (-4.46 <ycms mu mu< -2.96) and forward (2.03 <ycms mu mu< 3.53) rapidity regions. For the p-Pb collisions, the results are consistent within experimental and theoretical uncertainties with calculations that include both free-nucleon and nuclear-modified PDFs. For the Pb-Pb collisions, a 3.4<sigma> deviation is seen in the integrated yield between the data and calculations based on the free-nucleon PDFs, while good agreement is found once nuclear modifications are considered.

JOURNAL OF HIGH ENERGY PHYSICS 9, 76, 2020. DOI: 10.1007/JHEP09(2020)076

Eventos publicados

[P365-2020] "Bedside Optical Monitoring of Microvascular Reperfusion during Endovascular Thrombectomy"

Favilla, C. G.; **Forti, R. M.***; Baker, W. B.; Detre, J. A.; Kasner, S. E.; Kung, D.; Yodh, A. G.

ANNALS OF NEUROLOGY, Resumo do encontro: K-583, V. 88, SI, S95-S95, Supl. 25, 2020.

145th Annual Meeting American-Neurological-Association, De 04 a 09, Out. 2020, ELECTR NETWORK.

[P366-2020] "Executive summary"

Abi, B.; Acciarri, R.; Acero, M. A.; **Holanda, P. C. de*; Gelli, B.*; Guzzo, M. M.*; Kemp, E.*; Machado, A.*; Peres, O. L.*; Prakash, S.*; Reggiani-Guzzo, M.*; Segreto, E.*; Nunes, M. Soares*; Vanegas Forero, D.*; Vieira de Souza, H.***; et. al.; DUNE Collaboration

JOURNAL OF INSTRUMENTATION 15[8], T08008, 2020. DOI: 10.1088/1748-0221/15/08/t08008

***autores da comunidade IFGW.**
Fonte: Web of Science

Patentes

[Pa004-2020] "Sistema óptico baseado em fibras ópticas afinadas e método de medição de tração com alta sensibilidade"
Cristiano Monteiro de Barros Cordeiro; Claudecir Ricardo Biazoli
Número da Patente ou Registro: Agência INOVA PI1104345-8
Tipo: Patente de Invenção
Mês/Ano de Conclusão: 11/2020 - INPI/BRASIL

[Pa005-2020] "Processo de aglutinação de pós de materiais magnéticos, massa magnética assim obtida e uso em dispositivos termomagnéticos"
Adelino de Aguiar Coelho; Sergio Gama; Isaias da Silva
Número da Patente ou Registro: Agência INOVA BR 10 2012 012825 0
Tipo: Patente de Invenção
Mês/Ano de Conclusão: 11/2020 - INPI/BRASIL

[Pa006-2020] "Equipamento de Fluorescência de uma molécula só e seu uso"
Rene Afonso Nome; Juliano Grigoleto Hayashi; Cristiano Monteiro de Barros Cordeiro; Teresa Dib Zambon Atvars; Amanda Ferreira Costa
Número da Patente ou Registro: Agência INOVA BR 10 2014 009246 3
Tipo: Patente de Invenção
Mês/Ano de Conclusão: 12/2020 - INPI/BRASIL

Fonte: Sipex - Sistema de Informação de Ensino, Pesquisa e Extensão/Unicamp

Defesas de Teses do IFGW

[T015-2020] "Engenharia de Nanoestruturas Moleculares com Derivados de Porfirina em Superfícies Bem Definidas: O Papel da Interação Molécula-Substrato"
Aluno: Rodrigo Cezar de Campos Ferreira
Orientador: Prof. Dr. Abner de Siervo
Data: 27/11/2020

[T016-2020] "Decaimento Invisível e Visível de Neutrinos Solares"
Aluno: Renan Picoreti Nakahara
Orientador: Prof. Dr. Orlando Luis Goulart Peres
Data: 17/12/2020

Obs. Este período não houve defesas de Dissertações do IFGW.

Fonte: Portal IFGW/Pós-graduação - Agenda de Colóquios, Defesas e Seminários.
Disponível em: http://portal.ifi.unicamp.br/pos-graduacao

Defesas e Qualificações do PECIM

[Pe004-2020] "Conhecimento especializado do formador de professores que ensina teoria dos números para estudantes de licenciatura em matemática"
Aluno: Marieli Vanessa Rediske de Almeida
Orientador: Prof. Dr. Carlos Miguel da Silva Ribeiro
Data: 14/12/2020
Exame de Defesa: Doutorado
Banca: Prof. Dr. Carlos Miguel da Silva Ribeiro (orient.), Profa. Dra. Miriam Cardoso Utsumi FE / UNICAMP, Prof. Dr. Samuel Rocha de Oliveira IMECC / UNICAMP, Dr. Alessandro Jacques Ribeiro UFABC-Santo André, Dr. Luis Carlos Contreras González - UHU Universidad de Huelva, Profa. Dra. Laura Leticia Ramos Rifo - IMECC/Unicamp - suplente, **Prof. Dr. Gildo Girotto Júnior* - IFGW/Unicamp, suplente**, Dra. Myriam Codes Valcarce - UHU Universidad de Huelva, suplente.

[Pe005-2020] "Exame de qualificação - comunidade(s) de ciências da natureza no ensino médio, tensões e embates diante de um currículo por áreas"
Aluno: Paola Fernanda Guidi
Orientador: Profa. Dra. Maria Inês de Freitas Petrucci dos Santos Rosa
Data: 30/11/2020
Exame de Defesa: Mestrado
Banca: Profa. Dra. Maria Inês de Freitas Petrucci dos Santos Rosa (orientadora), Prof. Dr. Guilherme do Val Toledo Prado - FE/Unicamp, titular, Profa. Dra. Elisabeth Barolli - FE/Unicamp, titular, **Prof. Dr. Mauricio Urban Kleinke* - suplente**

[Pe006-2020] "Exame de qualificação - o desenvolvimento da cultura científica de estudantes de ensino médio em uma experiência de ensino não formal"
Aluno: André Luiz Polano Lucatelli
Orientador: Prof. Dr. José Joaquin Lunazzi
Data: 24/11/2020
Exame de Defesa: Doutorado
Banca: **Prof. Dr. José Joaquin Lunazzi* (orient.)**, Prof. Dr. Jorge Megid Neto FE / Unicamp , Dr. Marco Aurélio Alvarenga Monteiro - Faculdade de Engenharia de Guaratinguetá/ UNESP, Profa. Dra. Maria Cristina de Senzi Zancul - UNESP / Campus de Araraquara, suplente

Fonte: Página do PECIM - Programa de Pós-Graduação Multiunidades em Ensino de Ciências e Matemática – Mestrado e Doutorado (PECIM) da Unicamp.
Disponível em: https://www.pecim.unicamp.br/bancas

A Equipe da BIF deseja a todos
Feliz Natal
e um 2021 repleto de Esperança!

Abstracta

Instituto de Física
Diretor: Prof. Dr. Pascoal José Giglio Pagliuso
Diretora Associada: Profa. Dra. Mônica Alonso Cotta
Universidade Estadual de Campinas - UNICAMP
Cidade Universitária Zeferino Vaz
13083-859 - Campinas - SP - Brasil
e-mail: secdir@ifi.unicamp.br
Fone: +55 19 3521-5300

Publicação

Biblioteca do Instituto de Física Gleb Wataghin
http://portal.ifi.unicamp.br/biblioteca

Diretora Técnica: Sandra Maria Carlos Cartaxo
Coordenadora da Comissão de Biblioteca: Profa. Dra. Arlene Cristina Aguilar

Elaboração:
Maria Graciele Trevisan (Bibliotecária)
Ayres Neri da Cunha Junior (Técnico Administrativo)
contato: infobif@ifi.unicamp.br